A

Dissertation

on

Utilization of Agro-Food Waste Materials to Derive β-$Ca_2SiO_4:Eu^{3+}$ Phosphors for Near-UV Excited Light Emitting Diodes

Submitted in the partial fulfilment of the requirement for the award of degree of

Master of Science

in

Physics

(2017-2019)

Submitted by

Ishita Khurana

(301704013)

under the guidance of

Dr. O. P. Pandey

(Senior Professor)

School of Physics and Material Science,

Thapar Institute of Engineering & Technology,

Patiala (Punjab)-147004

CERTIFICATE

This is to certify that this dissertation entitled, **"Utilization of Agro-Food Waste Materials to Derive β-Ca_2SiO_4:Eu^{3+} Phosphors for Near-UV Excited Light Emitting Diodes"**, is submitted by **Ms. Ishita Khurana (301704013)** in fulfilment of requirement for the award of degree of Master of Science in Physics from School of Physics and Materials Science, Thapar Institute of Engineering & Technology, Patiala, India. It is an exclusive record of candidate's own research work under the supervision of **Dr. O.P. Pandey**. The dissertation in part or in full has not been submitted in any other university or institute for the award of any degree.

Dr. O.P. Pandey
Supervisor
Senior Professor
School of Physics and Materials Science
Thapar Institute of Engineering & Technology

DECLARATION

I hereby declare that the work presented in this thesis report entitled, **"Utilization of Agro-Food Waste Materials to Derive β-Ca_2SiO_4:Eu^{3+} Phosphors for Near-UV Excited Light Emitting Diodes"**, by me in partial fulfilment of requirement for the award of degree of **Master of Science** in **Physics** from School of Physics and Materials Science, Thapar Institute of Engineering & Technology, Patiala is an authentic award record on my work carried out under the supervision of **Dr. O.P. Pandey**, Senior Professor, School of Physics and Materials Science, Thapar Institute of Engineering & Technology, Patiala. The matter presented in this report has not been submitted in any other university or institute for award of Master of Science or any other degree.

Ishita Khurana

Ishita Khurana
Regd. No: 301704013

ACKNOWLEDGEMENT

At first, I would like to express my sincere thanks and deep gratitude to my M.Sc. dissertation thesis supervisor **Dr. O.P. Pandey** (Senior Professor, Head of Department, School of Physics and Material Science); a great philosopher and educator; for his expertise, review, assistance, guidance and patience throughout my research period. This dissertation would not have been possible without his guidance and words of encouragement. I thank him for giving such thoughtful feedback, always aimed at moving forward. He helped me to understand the intricate matters.

I acknowledge my gratitude to **Prof. Prakash Gopalan**, Director, Thapar Institute of Engineering & Technology, Patiala for providing all the necessary facilities for my research work.

I owe an enormous debt of gratitude to **Ms. Ruby Priya** for her sincere guidance, scholarly advice and passionate encouragement which made it possible to work on a topic that was of great interest to me. I thank her for embarking on this journey with me and staying with me till the end, no matter how I felt, she was there for me throughout. This work would not materialize without her prompt inspirations and timely suggestions. I would like to extend my thanks and appreciation to **Dr. Gurbinder Kaur** for her comprehensive advice. It is my privilege to thank all my labmates **Mr. Rameez Ahmad Mir**, **Mr. Aayush Gupta**, **Mr. Piyush Sharma**, **Ms. Damandeep Kaur**, **Mrs. Shivani Singla, Ms. Raveena Chaudhary**, **Mr. Sanjay Upadhaya,** and **Mr. Puneet Sharma**, for their invaluable help at every step during the project work.

I proudly take this opportunity to record heartiest thanks to my noble parents **Mr. Hargopal Khurana** and **Mrs. Reeta Khurana**, for their unconditional support, massive words of motivation, mellifluous affection and, blessings.

My final words go equally to all the concerned persons who have helped me willingly throughout this research work. It is the kindness of these acknowledged persons that this thesis sees the light of the day.

Above all, I thank the Almighty **GOD** for the wisdom, strength and gracious blessings he gave.

Ishita Khurana

Ishita Khurana

ABSTRACT

The sugar cane baggage ash and chicken shells are the abundant by-products of agro-food waste materials. These waste materials have hazardous impacts on the environment and thus it is a prerequisite to utilize these materials for the development of valuable products. The present report is a detailed study to use these materials to fabricate intense red-light emitting Eu-doped Ca_2SiO_4 phosphors via conventional solid-state method. For this purpose, silica (SiO_2) is extracted from sugarcane baggage ash at 600 ℃ via alkali extraction followed by acid precipitation method. The raw eggshells were washed, dried and calcined in the furnace at 900 ℃ in order to get calcium oxide (CaO). The structural, morphological, elemental, optical and luminescent properties were characterized via X-ray diffraction (XRD), scanning electron microscopy (SEM), energy dispersed X-ray spectroscopy (EDX), UV-Visible spectroscopy (UV-Vis), Fourier transformed infrared spectroscopy (FT-IR) and photoluminescence (PL) techniques. The effect of Eu concentration (0.1 to 0.5 mol%) on the structural, optical and luminescent properties of Ca_2SiO_4 has been studied in details. The agro-food waste derived phosphors exhibited intense emission at 625 nm corresponding to $^5D_0 \rightarrow {}^7F_2$ transitions of Eu^{3+} ions under near UV-light excitation at 393 nm. The quenching mechanism and type of energy transfer interactions involved are studied via Blasse and Dexter's theory. The photometric parameters such as CIE co-ordinates, CCT values, and color purity are calculated from emission spectra. The present agro-food waste derived phosphors are expected to be promising candidates for near UV-excited white light emitting diodes in solid-state lighting and optoelectronic devices.

List of Figures

List of Tables

Page

Chapter 2

Chapter 6

Table of contents

CHAPTER 1
INTRODUCTION

1.1. Luminescence

'Luminescence' is a process where a substance absorbs a particular kind of energy from an outside source and re-emits that energy as light [1]. This release of light energy takes place from electronic excited states without involving heat and is therefore called cold emission. Here, the word *light* includes visible light (400-750 nm) as well as the neighboring locales on both the extremities, which are near-ultraviolet and near-infrared zones [2]. The produced radiation is emitted with a frequency depending on the energy gap between the lower and higher energy states. Initially, a German scientist named Eilhard Wiedemann utilized this word 'luminescence' in 1888. It was derived from a Latin word called *lumen*, which translates to light.

1.2. Types of luminescence:

Luminescence can be stimulated by chemical reactions, electric field, UV or visible light, energetic electrons, subatomic movements, or pressure on a crystal. Based on the kind of excitation source used, luminescence can be classified as follows:

i. Bioluminescence – Light is emitted by living organisms as an aftereffect of a chemical reaction. It is essentially a sort of chemiluminescence. e.g. fireflies produce a chemical luciferin which reacts with oxygen to generate light.

ii. Chemiluminescence – The emission of light takes place as a result of chemical or electrochemical reactions. e.g. glowstick.

iii. Electroluminescence – Light is generated because of the excitation of atoms or molecules of a material by an applied electromagnetic field. e.g. light emitting diodes.

iv. Cathodoluminescence – The emission of light takes place when a beam of electrons generated from an external source interacts with luminescent material. e.g. cathode ray tubes used earlier to make displays.

v. Photoluminescence – This involves excitation of atoms or molecules of a substance by the absorption of photons. Depending on the nature of the excited state, photoluminescence is divided into two types as explained below:

a) Fluorescence:

Fluorescence is the process where light is emitted from a singlet excited state. It involves instantaneous re-emission of the absorbed light by the substance. Light emission ceases suddenly on the removal of the excitation source. e.g. fluorescent light bulbs.

b) Phosphorescence:

The release of light from a triplet energized state is called phosphorescence. It involves delayed re-emission of the absorbed light by the substance. The glow of phosphorescence may persist for several seconds up to a few days after the removal of excitation source and is therefore termed as afterglow. e.g. glow in the dark toys generally made up of phosphor materials like zinc sulfide and strontium aluminate.

The schematic mechanism of fluorescence and phosphorescence phenomena is shown in Fig.1.1.

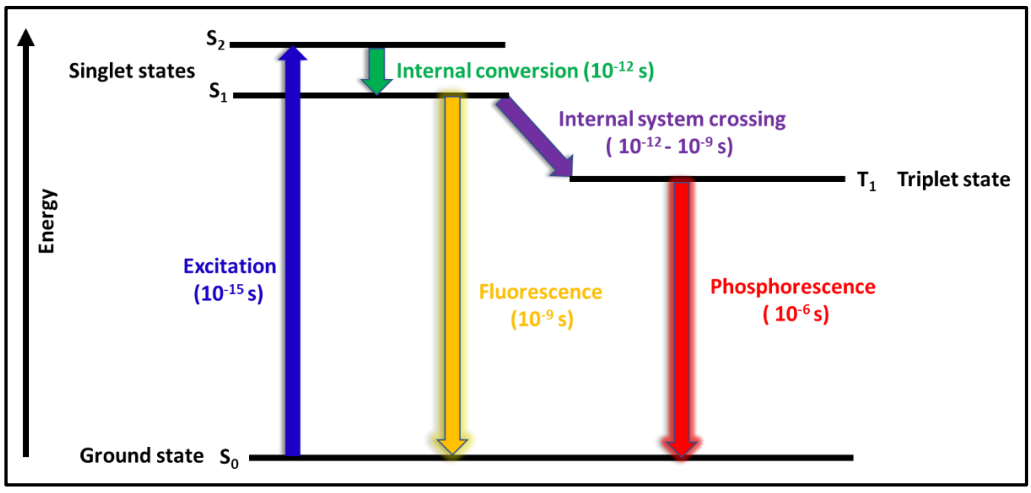

Figure 1.1: Fluorescence and phosphorescence mechanism in a substance

vi. Mechanoluminescence – Light emission is caused by mechanical action acted upon a solid material. It may produce elastic deformation or may rupture the bonds of the material.

vii. Thermoluminescence – The emission of light caused upon heating of certain crystalline materials previously excited by ionizing radiation (UV rays, X-rays, γ-rays, β-rays, etc.). The heat provided releases trapped electrons in a substance.

viii. Sonoluminescence – The discharge of extreme light energy in short bursts when the bursting bubbles in a fluid are energized by sound energy.

1.3. Key elements of phosphors: Activators and Sensitizers

The substances which produce visible light upon interaction with different radiations like ultraviolet, X-rays, electron beam, infrared radiations, etc. are known as 'Phosphors' [3]. 'Phosphor' is a Greek word which means 'light bearer' [2]. Primarily, phosphors are made out of a transparent microcrystalline host and a luminescent center often called an activator as shown in fig. 1.2 (a). An activator is a small amount of intentionally added impurity element to the host crystal. There are various types of activators depending on their interaction with the host lattice. Lanthanide ions such as Eu^{3+} interact weakly with host lattice undergoing f-f transitions whereas the d electrons of Eu^{2+} interact strongly with the lattice [4]. The host is treated only as a medium for the activator. The host materials can be nitrides, sulfides, silicates, oxides, selenides, halides, etc. In the luminescence process in a phosphor material, the incident radiation is absorbed by the activator atoms and are excited to higher energy levels. Finally, the excited atoms come back to the ground state by means of a mix of radiative and non-radiative emission. The activator ions convert the absorbed energy into a useful frequency of visible light producing radiative emission. Hence, only a trace of dopant atoms called emission centers radiate in luminescence. The non- radiative losses dissipated as heat energy excites the vibrations of the host lattice. The suppression of non-radiative emission is necessary to increase the efficiency and quantum yield of luminescent materials. In some phosphors, the activator ions cannot be excited because of forbidden transitions. The incident radiation is retained by the especially added ions which is subsequently transferred to the activator. In this scenario, these absorbing ions are called as sensitizers [5]. Therefore, the luminescence processes of a phosphor mainly depend on the processes related to the host and those that occur around and within the activator. Fig. 1.2 (b) diagrammatically illustrates the role of activator and sensitizer in luminescent materials.

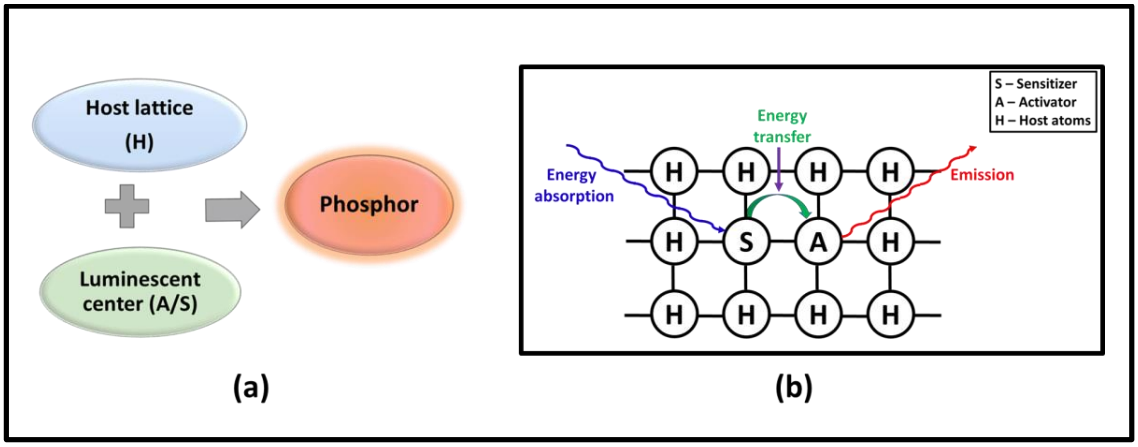

Figure 1.2: (a-b) Demonstrates the composition of phosphor and the luminescence phenomenon via transfer of energy from the sensitizer to the activator

1.4. Need of white light emitting diodes

(SSL) Solid-state lightening has evolved as another refined innovation with its ultimate potential to be smart and ultra-efficient [6]. SSL is a technology in which LEDs (light-emitting diodes), OLEDs (organic light emitting diodes), or light producing polymers replace conventional incandescent or fluorescent lights, where light was produced from gaseous substances enclosed in a bulb. Solid-state lightening produces visible light by means of electroluminescence, a non-thermal process which creates light by the excitation of high energy electrons in phosphor materials. Therefore, at present, the usage of phosphor materials is evolving at an amazing pace. Compared with conventional illumination, LEDs offer several advantages such as low electric consumption, life beyond 10000 hr, ease in color rendering, no burn-out, reduced sensitivity to variation and less heat generation [7–10]. Typically, white illumination is achieved by the blend of a blue LED and yellow light producing phosphor ($Y_3Al_5O_{12}:Ce^{3+}$) [8,11]. The conversion of blue light generated in the LED into yellow light takes place in the layer of phosphor material. The mixture of visible blue and yellow light provides the desired white illumination. Nevertheless, this white light produced suffers from the downsides of less color rendering index (CRI) and higher correlated color temperature (CCT) because of the absence of red constituent [12]. The warm white light preferred for home lighting applications can be produced by including a red light producing phosphor and employment of broad-spectrum phosphors. Alternatively, a blend of green and red phosphors with a blue LED chip can also generate white light [13]. But, due to the poor heat-resistance of conventional red phosphors, the

intensity of lumination depletes [14]. Therefore, to bring advancement in LED technology, it is crucial to produce efficient red emitting phosphor materials with excellent color stability and high luminous efficacy [15].

1.5. Agro-food wastes for phosphor materials

In recent times, the conversion of agro-food wastes into low-cost luminescent materials has gained significant attention [16]. Increasing urbanization and population growth rate accounts for the considerably large production of agro-food wastes across the world [17]. Crop residues, poultry houses, farm remains, manure of animals produces a huge amount of agro-food wastes. Animal manure and other horticultural solid by-products are discharged to the landfills. This leads to the release of lethal gases and debases the environmental sources [18]. These wastes have a drastic impact on soil quality, land fertility and, human health. Therefore, it is necessary to explore effective waste utilization ways to minimize environmental hazards [19]. Agro-food wastes are widely used in brick making, fodder, biodiesel, fertilizers, fillers, adsorbents, and energy production. In the quest of utilizing agro-food wastes for various applications, researchers have made attempts to use these materials for the development of phosphors. The commonly used agro-food waste materials are chicken egg shell, rice husk ash, sugarcane leaves, sugarcane bagasse ash, bamboo leaves, etc.

Sugarcane is one of the most cultivated crops across Asian countries. Sugarcane is used for the extraction of jaggery, sugar and alcoholic beverages from its juice. The bagasse left behind is burnt out as a source of fuel in the local field areas [20]. The ash disposal methods lead to public health hazards and environmental threats due to mismanagement of waste [21]. On the other hand, several studies have investigated high silica (SiO_2) contents in bagasse ash. The silica content in bagasse ash is more than 60-70 % and is considered as a fine source for the synthesis of amorphous silica [18,22,23]. The amount of silica depends upon the type of soil and harvesting [24]. Silica in its finest form is used in ceramics, glass, functional filler for paints, thermal insulation, biomedical, rubber industry, and optoelectronic devices [25–27].

While the chicken eggshells are another category of agricultural waste material having relatively small utilization. Poultry, bakeries, homes, hotels, and food production industries are various sources of solid eggshell waste [28–30]. The dumping of eggshells

to landfills without any earlier treatment produces a harmful impact on the environment. Most recent research has explored the applications of eggshells, for example, eggshell based compost, concrete added substance and natural adsorbent of metal with high adsorption capacity [31]. Eggshells are a rich source of calcium carbonate ($CaCO_3$) [32]. They have a high calcium content typically above 90 % [33–35]. $CaCO_3$ can be easily converted into CaO after calcination at temperature approximately from 850 to 950 ℃ [36]. These two agricultural wastes can be utilized for the synthesis of calcium silicate phosphors using CaO and SiO_2 as precursors. The salient features of CaO, SiO_2 and, calcium silicates are explained as below:

1.5.1. Silica (SiO_2, silicon dioxide)

Pure silicon found in nature is too reactive and hence combines either with oxygen as silica or with oxygen and other elements like aluminium, magnesium, calcium, sodium, potassium, or iron as silicates. Silicates form a large number of different phases due to the diversity of their structure. Silica (SiO_2) is one of the most important and abundant materials [37].

1.5.1.1. Types of Silica

I. Crystalline silica

SiO_2 has a number of distinct crystalline forms. Majority of the crystalline structures include tetrahedral SiO_4 units connected together by common vertices in various configurations [38]. Quartz polymorphs are one of the widely known examples.

***a)* α quartz (high-temperature quartz)**

It belongs to the trigonal crystal system. The bond length of Si-O bond in α-quartz is 0.162 nm. Also, the angle corresponding to Si-O-Si is 146-155º.

***b)* β quartz (low-temperature quartz)**

It crystallizes in the hexagonal crystal system. The bond length of Si-O bond is 0.160-0.162 nm. Moreover, the angle attributed to Si-O-Si is 143-147º. The conversion of α-quartz to β-quartz happens unexpectedly at 573 ℃.

II. Amorphous silica

In amorphous silica, all four oxygen atoms of silicate are shared with other silicon atoms forming a three-dimensional structure of SiO_2. e.g. glass. Fig. 1.3 represent the structures of crystalline and amorphous silica.

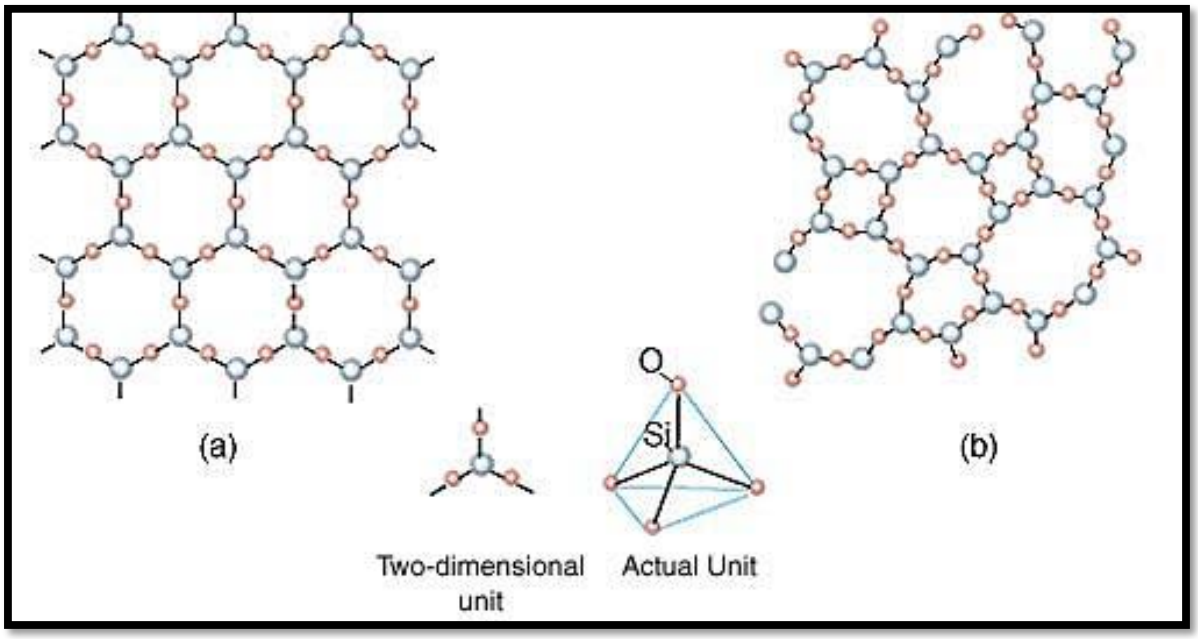

Figure 1.3: (a-b) shows the crystalline and amorphous structure of SiO_2, respectively [39,40].

1.5.1.2. Properties of silica

(a) Properties of Silica Glass

i. Silica glass is a non-crystalline amorphous substance.

ii. They are typically fragile and visually transparent.

iii. It can refract, reflect, and transmit light in accordance with the fundamentals of optical science.

iv. Silica glass has the potential to emit color by the inclusion of charged ions.

(b) Properties of Quartz

i. Quartz crystals build up an electric potential when mechanical force is applied. Therefore, they show piezoelectric characteristics.

ii. Pure quartz is usually colorless and is transparent or translucent. Opaque crystals are usually micro-sized while transparent crystals are macro-sized. The presence of

contaminants in the crystal produces color. As for example, **rose quartz** – Silica added with small amounts of iron generates a pinkish effect.

iii. Quartz crystals are hard materials with a 7 rating on the **Mohs scale**.

iv. The melting and boiling points of silica are very high; 1710 ℃ and 2230 ℃, respectively.

v. The reaction of silica with various metal oxides such as lead oxide or sodium oxide produces different types of glasses like borosilicate glass or lead glass.

1.5.2. Calcium Silicates

Calcium silicates are chemical compounds composed of CaO and SiO_2. They are prepared by calcining the oxide with silica, SiO_2, at elevated temperatures.

1.5.2.1. Types of calcium silicates

The calcium silicates exist in various forms in nature. However, calcium silicates exist in three major forms:

i. $CaSiO_3$ (monosilicate)

ii. $Ca_3Si_2O_7$ (disilicate)

iii. Ca_2SiO_4 (orthosilicate)

1.5.2.2. Structure of calcium silicates

i. $CaSiO_3$

In $CaSiO_3$, CaO and SiO_2 are present in 1:1 mole ratio. It has a perovskite structure. The $CaSiO_3$ polymorphs are differentiated on the basis of the sort of polymerization of silicate tetrahedral [41].

a) **Wollastonite (wol, α- $CaSiO_3$)**

It is a polymorph formed at high-temperature conditions. The crystal structure includes covalent bonding of three tetrahedra of silicate forming a ring structure.

b) **Pseudowollastonite (psw, β- $CaSiO_3$)**

This polymorph is also known as pseudo-wol and is formed at low-temperature conditions. A chain is formed via sharing of silicate tetrahedra at the corners.

ii. $Ca_3Si_2O_7$

$Ca_3Si_2O_7$ is also known as rankinite. In the structure of rankinite, two silicon-oxygen tetrahedra are linked to form a unit (Si_2O_7 groups). The groups are linked together by Ca and each has seven nearest neighbors of oxygen atoms. The Ca-O bond length is in the range from 2.25 to 2.90 Å. The angles of O-Ca-O are from 60 to 87º. The Si_2O_7 groups

have nearly regular tetrahedra, like other silicates. The bond length Si-O is in the range from 1.52 to 1.65 Å. The angles of O-Si-O are from 106 to 115º. This value is larger than Si_2O_7 tetrahedra of other silicates. The crystal structure of rankinite is monoclinic [42]. The lattice parameters are: a = 10.60 Å, b = 8.92 Å, c = 7.89 Å, β = 119.6º.

iii. Ca_2SiO_4

The basic structure of all the phases of Ca_2SiO_4 consists of a sub-structure of interconnected calcium polyhedra and isolated silicate tetrahedra [SiO_4]. It exists in five phases α_L, α_H, α, β, and γ as described below [43–46]:

***a)* γ phase (low-temperature phase)**

The γ phase exhibits an orthorhombic and olivine sort of a structure. This phase is most reliable at room temperature.

***b)* β phase (low-temperature phase)**

The structure of β phase is monoclinic. It can be derived from α_l phase via cooling.

***c)* α phase (high-temperature phase)**

The structure of α phase is not yet predicted precisely. However, several suggestions reveal the existence of trigonal or hexagonal structure. It is an orientationally disordered structure with space group P63 /mmc.

***d)* α_L phase (high-temperature phase)**

Basically, the orthorhombic α_H phase is a sub-structure of this phase which leads to two dissimilar possibilities. First, the parameters a and c of the α_H phase are doubled in α_L phase. Secondly, the thrice of β parameter of the α_H phase may take place.

***e)* α_H phase (high-temperature phase)**

The α_H phase has β-K_2SiO_4 structure.

1.5.2.3. Properties of calcium silicates

i. Calcium silicate is a freely-flowing white powder.

ii. It can be derived from the chemical reaction of calcium oxide and silica in different proportions.

iii. They show high absorption of water and less density.

iv. They are efficient luminescent materials because of their low cost, stable crystal structure, long term stability and, wide transparency.

v. It is used in roads, bricks, roof tiles, table salt and, even therapeutic antacids.

vi. It's chemical constitution makes it especially suitable as a prime ingredient in high-temperature insulation.

1.6. Calcium silicates as phosphor materials

The selection of host matrix for phosphors materials is a vigilant task. Wide optical band gap, better stability and, good solubility are some of the significant characteristics of the host matrix. Silicates have been an excellent host matrix due to their low cost, stable crystal structure with a powerful absorption in the near-UV region [47–50]. Various silicates accommodate different cations to stabilize the charge of the fundamental structural unit. The substitution of silicon atoms by appropriate atoms is also feasible. Among silicate-based hosts, calcium silicates prove to be a highly versatile luminescent host due to their unique physical, chemical and optical properties [51,52]. The introduction of various guest ions in this host lattice may generate a broad range of multiple color emission spectra. The tetrahedral silicate (SiO_4^{2-}) ion offers high mechanical resistance and stability. Calcium silicates are efficient luminescence yielding phosphors as they exhibit high thermal strength, good conductive properties, higher thermal stability and are chemically inert [53]. Moreover, calcium silicates require facile synthesizing conditions. The fabrication of these phosphors is relatively inexpensive due to low price and abundance of calcium and silica [54]. In addition, Ca_2SiO_4 is a promising host matrix because of its broad band gap and outstanding chemical, physical and thermal properties. The structure of Ca_2SiO_4 possesses two different Ca sites with coordination of seven and eight oxygens, denoted by Ca(I) and Ca(II) sites, respectively. The dopant atom may substitute any of these two Ca sites in the host lattice. In case of Ca_2SiO_4:Eu, Eu^{3+} ions preferentially substitute any of two Ca sites and influence the luminescence properties. Eu^{3+} is an efficient red light emitting dopant due to its sharp, narrow, characteristic emission peaks. The present report deals with the synthesis of Eu doped Ca_2SiO_4 phosphors via conventional solid-state method. In this approach, the precursors are extracted from agro-food waste materials.

REFERENCES

[1] J.R. Lakowicz, Principles of Fluorescence Spectroscopy, 3rd ed., Springer Science and Business Media, LLC, (2006).

[2] E.M.J. Weber, A.A. Kaminskii, M.J. Weber, M.J. Weber, M.J. Weber, Phosphor Laser and Optical Science and Technology Series Physics and Chemistry of Photochromic Glasses, (2006).

[3] T. Watari, T. Tsuji, K. Mori, H.N. Luitel, T. Torikai, M. Yada, C.N. Xu, T. Terasaki, Fabrication and Characterization of Calcium Silicate Phosphors - Ca_2SiO_4 and Ca_2MgSiO_7 -, Mater. Sci. Forum. 761 (2013) 59–64.

[4] A. Mayavan, J. Ganesamurthi, S. Gandhi, Templated synthesis and characterization of red emitting $Ca_{1-x}Sr_{1-x}Eu_{2x}^{3+}SiO_4$ phosphor for LED applications, Bulletin of Materials, 41 (2017) 121-126.

[5] G.Blasee, B. C. Grabmaier-Luminescent Materials -Springer-Verlag (1994).

[6] Z.Y. Mao, Y.C. Zhu, Y. Zeng, L. Gan, Y. Wang, Concentration quenching and resultant photoluminescence adjustment for $Ca_3Si_2O_7:Tb^{3+}$ green-emitting phosphor, J. Lumin. 143 (2013) 587–591.

[7] H. Ju, L. Wang, B. Wang, Y. Ma, H. Wang, S. Chen, X. Tao, Single-phased emission-tunable $Ca_3Si_2O_7:Ce^{3+}$, Eu^{2+} phosphors for white light-emitting diodes, Ceram. Int. 39 (2013) 8001–8005.

[8] W. Lv, N. Guo, Y. Jia, Q. Zhao, H. You, A potential single-phased emission-tunable silicate phosphor $Ca_3Si_2O_7:Ce^{3+}$, Eu^{2+} excited by ultraviolet light for white light emitting diodes, Opt. Mater. (Amst). 35 (2013) 1013–1018.

[9] C.H. Huang, W.R. Liu, T.S. Chan, Y.T. Lai, Orangish-yellow-emitting $Ca_3Si_2O_7:Eu^{2+}$ phosphor for application in blue-light based warm-white LEDs, Dalt. Trans. 43 (2014) 7917–7923.

[10] M. Venkataravanappa, H. Nagabhushana, G.P. Darshan, B. Daruka Prasad, G.R. Vijayakumar, H.B. Premkumar, Udayabhanu, Novel EGCG assisted ultrasound synthesis of self-assembled $Ca_2SiO_4:Eu^{3+}$ hierarchical superstructures: Photometric characteristics and LED applications, Ultrason. Sonochem. 33 (2016) 226–239.

[11] H. Tian, J. Song, Q. Fei Lu, D. Jian Wang, Flux-adjusted phase transformation from Ca_2SiO_4 to $Ca_3Si_2O_7$ with Eu^{2+} activator for white light emitting diodes, Optoelectron. Lett. 8 (2012) 352–355.

[12] Z.Y. Mao, Y.C. Zhu, Y. Wang, L. Gan, Ca_2SiO_4:Ln (Ln = Ce^{3+}, Eu^{2+}, Sm^{3+}) tricolor emission phosphors and their application for near-UV white light-emitting diode, J. Mater. Sci. 49 (2014) 4439–4444.

[13] Z.Y. Mao, Y.C. Zhu, L. Gan, Y. Zeng, F.F. Xu, Y. Wang, H. Tian, J. Li, D.J. Wang, Tricolor emission $Ca_3Si_2O_7$:Ln (Ln = Ce, Tb, Eu) phosphors for near-UV white light-emitting-diode, J. Lumin. 134 (2013) 148–153.

[14] F. Qian, R. Fu, S. Agathopoulos, X. Gu, X. Song, Synthesis and luminescence properties of a broad-band red phosphor $Ca_3Si_2O_7:Eu^{2+}$ for warm white light-emitting diodes, J. Lumin. 132 (2012) 71–75.

[15] K. Mondal, D.K. Singh, J. Manam, Spectroscopic behavior, thermal stability and temperature sensitivity of Ca_2SiO_4: Eu^{3+} red emitting phosphor for solid-state

lighting application, J. Alloys Compd. 761 (2018) 41–51.
[16] L.L. Devi, C. Basavapoornima, V. Venkatramu, C.K. Jayasankar, J. Kaewkhao, W. Lertlop, Structural and luminescence properties of Sm^{3+}-doped Ca_2SiO_4 phosphors from agricultural waste, Mater. Today Proc. 5 (2018) 15081–15085.
[17] S. Punj, K. Singh, Blue-green light emitting inherent luminescent glasses synthesized from agro-food wastes, J. Mater. Sci. Mater. Electron. 30 (2019) 3871–3881.
[18] N. Sapawe, N. Surayah Osman, M. Zulkhairi Zakaria, S. Amirul Shahab Syed Mohamad Fikry, M. Amir Mat Aris, Synthesis of green silica from agricultural waste by sol-gel method, Mater. Today Proc. 5 (2018) 21861–21866.
[19] L.L. Devi, C. Basavapoornima, V. Venkatramu, P. Babu, C.K. Jayasankar, Synthesis of Ca_2SiO_4:Dy^{3+} phosphors from agricultural waste for solid-state lighting applications, Ceram. Int. 43 (2017) 16622–16627.
[20] J.S. Le Blond, C.J. Horwell, B.J. Williamson, C. Oppenheimer, Generation of crystalline silica from sugarcane burning, J. Environ. Monit. 12 (2010) 1459–1470.
[21] C. Channoy, S. Maneewan, C. Punlek, S. Chirarattananon, Preparation and Characterization of Silica Gel from Bagasse Ash, Adv. Mater. Res. 1145 (2018) 44–48.
[22] Nazriati, H. Setyawan, S. Winardi, Synthesis of silica aerogel from bagasse ash by ambient pressure drying, AIP Conf. Proc. 1415 (2011) 114–116.
[23] V. Vaibhav, U. Vijayalakshmi, S.M. Roopan, Agricultural waste as a source for the production of silica nanoparticles, Spectrochim. Acta - Part A Mol. Biomol. Spectrosc. 139 (2015) 515–520.
[24] P. Worathanakul, W. Payubnop, A. Muangpet, Characterization for Post-treatment Effect of Bagasse Ash for Silica Extraction, Int. J. Chem. Mol. Nucl. Mater. Metall. Eng. 3 (2009) 339–341.
[25] R. Yuvakkumar, V. Elango, V. Rajendran, N. Kannan, High-purity nano silica powder from rice husk using a simple chemical method, J. Exp. Nanosci. 9 (2014) 272–281.
[26] L.L. Devi, C.K. Jayasankar, Spectroscopic investigations on high efficiency deep red-emitting Ca_2SiO_4:Eu^{3+} phosphors synthesized from agricultural waste, Ceram. Int. 44 (2018) 14063–14069.
[27] R.H. Alves, T.V.D.S. Reis, S. Rovani, D.A. Fungaro, Green Synthesis and Characterization of Biosilica Produced from Sugarcane Waste Ash, J. Chem. 2017 (2017) 1-9.
[28] S. Sethupathi, C. Kai, L. Loong Kong, Y. Munusamy, M.J. Khalil Bashir, N. Iberahim, Malaysian journal of analytical sciences, Preliminary study of sulfur dioxide removal using calcined eggshell, Malaysian J. Anal. Sci. 21 (2017) 719–725.
[29] T. Witoon, Characterization of calcium oxide derived from waste eggshell and its application as CO_2 sorbent, Ceram. Int. 37 (2011) 3291–3298.
[30] Y.C. Wong, R.X. Ang, O. Access, Study of calcined eggshell as potential catalyst for biodiesel formation using used cooking, Open Chemistry 16 (2018) 1166–1175.
[31] S. Ummartyotin, B. Tangnorawich, Utilization of eggshell waste as raw material for synthesis of hydroxyapatite, Colloid Polym. Sci. 293 (2015) 2477–2483.
[32] L.M. Correia, R.M.A. Saboya, N. de Sousa Campelo, J.A. Cecilia, E. Rodriguez-

Castellon, C.L. Cavalcante, R.S. Vieira, Characterization of calcium oxide catalysts from natural sources and their application in the transesterification of sunflower oil, Bioresour. Technol. 151 (2014) 207–213.
[33] F. Luna Vera, M. Guancha Chalapud, I. Castillo Viveros, E.A. Vasquez Medina, From Eggshells to Quicklime: Using Carbonate Cycle as an Integrating Concept to Introduce Students to Materials Analysis by TGA and FTIR, J. Chem. Educ. 95 (2018) 625–630.
[34] N. Tangboriboon, R. Kunanuruksapong, A. Sirivat, R. Kunanuruksapong, A. Sirivat, Preparation and properties of calcium oxide from eggshells via calcination, Mater. Sci. Pol. 30 (2012) 313–322.
[35] H.D. Jirimali, B.C. Chaudhari, J.C. Khanderay, S.A. Joshi, V. Singh, A.M. Patil, V. V. Gite, Waste Eggshell-Derived Calcium Oxide and Nanohydroxyapatite Biomaterials for the Preparation of LLDPE Polymer Nanocomposite and Their Thermomechanical Study, Polym. - Plast. Technol. Eng. 57 (2018) 804–811.
[36] T. Andherson, D. Rachmat, D.D. Risanti, Potential use of chicken eggshells and cacao pod husk as catalyst for biodiesel production, AIP Conf. Proc. 1945 (2018).
[37] N. Rahmat, M.A. Sabali, A.V. Sandu, N. Sahiron, I.G. Sandu, Study of Calcination Temperature and Concentration of NaOH Effect on Crystallinity of Silica from Sugarcane Bagasse Ash (SCBA), Rev. Chim. 67 (2016) 1872–1875.
[38] R. Bruckner, Properties and structure of vitreous silica, Journal of non-crystalline solids 5 (1970) 123-175.
[39] M. Moreno, M. Domínguez, R. Ambrosio, A. Torres, A. Torres, P. Rosales, A. Itzmoyotl, Amorphous, Polymorphous, and Microcrystalline Silicon Thin Films Deposited by Plasma at Low Temperatures, Cryst. Non-Crystalline Solids. (2016).
[40] I. Benigno, D. Darminto, Effect of Intrinsic Layer Energy Gap and Thicknesses Optimization on the Efficiency of p-i-n Amorphous Silicon Solar Cell, IPTEK J. Sci. 2 (2017) 2337-8350.
[41] N. Zhang, J.A. Molenda, S. Mankoci, X. Zhou, W.L. Murphy, N. Sahai, Crystal structures of $CaSiO_3$ polymorphs control growth and osteogenic differentiation of human mesenchymal stem cells on bioceramic surfaces, Biomater. Sci. 1 (2013) 1101–1110.
[42] I. Kusachi, C. Henmi, A. Kawahara, K. Henmi, The structure of rankinite, Mineral. J. 8 (1975) 38–47.
[43] N.A. Yamnova, N. V. Zubkova, N.N. Eremin, A.E. Zadov, V.M. Gazeev, Crystal structure of larnite β-Ca_2SiO_4 and specific features of polymorphic transitions in dicalcium orthosilicate, Crystallogr. Reports. 56 (2011) 210–220.
[44] J. Liu, C.G. Duan, W.N. Mei, R.W. Smith, J.R. Hardy, Polymorphous transformations in alkaline-earth silicates, J. Chem. Phys. 116 (2002) 3864–3869.
[45] F. Gfeller, R. Widmer, B. Kruger, E. V. Galuskin, I.O. Galuskina, T. Armbruster, The crystal structure of flamite and its relation to Ca_2SiO_4; polymorphs and nagelschmidtite, Eur. J. Mineral. 27 (2015) 755–769.
[46] J. Barbier, B.G. Hyde, The structures of the polymorphs of dicalcium silicate, Ca_2SiO_4, Acta Crystallogr. Sect. B. 41 (1985) 383–390.
[47] D. V. Sunitha, H. Nagabhushana, S.C. Sharma, B.M. Nagabhushana, R.P.S. Chakradhar, Luminescent characteristics of Eu^{3+} doped di-calcium silicate nano-powders for white LEDs, J. Alloys Compd. 575 (2013) 434–443.

[48] M.O. Onani, F.B. Dejene, Photo-luminescent properties of a green or red emitting Tb^{3+} or Eu^{3+} doped calcium magnesium silicate phosphors, Phys. B Condens. Matter. 439 (2014) 137–140.
[49] A. Baran, J. Barzowska, M. Grinberg, S. Mahlik, K. Szczodrowski, Y. Zorenko, Binding energies of Eu^{2+} and Eu^{3+} ions in β-Ca_2SiO_4 doped with europium, Opt. Mater. (Amst). 35 (2013) 2107–2114.
[50] E. Ozturk, E. Karacaoglu, The Effect of Ligand-To-Eu^{3}+ Charge-Transfer Transitions (Lmct) on the Photoluminescence Intensity of M_2SiO_4: Eu^{3+} (M = Ca, Zn) Type Phosphors, Mater. Sci. Pol. 36 (2018) 509–513.
[51] S.Verma, A. Mishra, M. Bhuie, N.K. Singh, Comparative analysis of luminescence Property of Tb^{3+} and Er^{3+} Activated Calcium Silicate Phosphor, International Journal of Computer Science and Engineering, 6 (2018) 108-114.
[52] R. Dai, C. Tong, Y. Zhu, C. Xu, L. Yang, Y. Li, Mineralization and optical properties of Eu^{3+}- doped tricalcium silicate soaked in dilute K_2HPO_4 aqueous solution, Opt. Mater. (Amst). 85 (2018) 32–40.
[53] H. Nagabhushana, B.M. Nagabhushana, M. Madesh Kumar, Chikkahanumantharayappa, K.V.R. Murthy, C. Shivakumara, R.P.S. Chakradhar, Synthesis, characterization and photoluminescence properties of $CaSiO_3$:Eu^{3+} red phosphor, Spectrochim. Acta - Part A Mol. Biomol. Spectrosc. 78 (2011) 64–69
[54] D. Stefanska, P.J. Deren, Luminescence investigation and thermal stability of blue-greenish emission generated from $Ca_3MgSi_2O_8$:Eu^{2+} phosphor, Opt. Mater. (Amst). 80 (2018) 62–64.

CHAPTER- 2

LITERATURE SURVEY

In order to synthesize calcium silicate from agro-food wastes, a peer-review survey of literature has been done. The primary aim of the present study is to synthesize calcium silicate phosphors utilizing agro-food waste materials. For this purpose, a peer review of the existing literature has been done. The important findings reported by researchers are outlined in the chronological order:

2.1. Literature survey of silica from agro-food waste

Nazriati *et al.* [1] in **2011** prepared silica aerogels using bagasse waste. The method adopted was (APD) ambient pressure drying. Firstly, a sodium silicate solution was formed from bagasse ash by alkali extraction method. Then, the ash was treated with 2N solution of NaOH along with 1 hr of steady stirring. Silica was chemically treated with alkyl group. The Brunauer–Emmett–Telle (BET) results revealed the high surface of as-synthesized silica aerogels at around 450.2 to 1360.4 m^2/g. Porous volume was found to be in the range from 0.7 to 1.9 cm^3/g.

Yuvakkumar *et al.* [2] in **2012** obtained silica via alkali and acid treatment technique. Rice husk waste was used to extract silica powder. Sodium hydroxide (NaOH) purification treatment with varying concentrations of NaOH (0.5, 1, 1.5, 2 and 2.5 N) was done to extract nano-silica powder. Silica was derived with a maximum purity of 99.9 % at NaOH concentration of 2.5 N. Various characterization techniques were performed such as energy-dispersive spectroscopy (EDX), Fourier transform infrared spectroscopy (FTIR), X-ray diffraction (XRD), transmission electron microscopy (TEM), particle size determination and BET analysis. The particle size on an average was estimated to be 25 nm.

Usman *et al.* [3] in **2014** reported extraction of silica from sugarcane bagasse. The bagasse samples were given heat treatments at three different temperatures 500, 600 and 700 ℃, respectively in order to remove moisture and other light impurities. After burning, the ash percentages were found to be 12.65, 10.89 and 9.95 %, respectively. The percentage of oxide constituents was measured by performing X-ray fluorescence (XRF). XRF results

illustrated that the silica contents were 76.17, 76.29 and 77.286 %, respectively. The high silica content in the bagasse ash revealed its potential application as reinforcement.

Vaibhav *et al.* [4] in **2015** carried out a study to determine the silica content from four different waste materials. The sources used were bamboo leaves, rice husk, groundnut shell and, sugarcane bagasse. These waste products were calcined at 900 ℃ for 7 hrs to remove volatile impurities. The obtained samples were continuously stirred along with NaOH chemical treatment. The product finally formed was a solution of sodium silicate. Further, acid precipitation of silica was done using 6 M H_2SO_4. The amount of silica extracted from various sources was: Rice husk – 78 %, Sugarcane bagasse – 71 %, Groundnut shell – 5.52 % and Bamboo leaves – 52%, respectively.

Rahmat *et al.* [5] in **2016** synthesized silica from bagasse ash by acid washing and acid leaching treatment. The bagasse samples were stirred and boiled in different concentrations of sodium at 3 M and 4 M, respectively to extract silica. The calcinated ash was characterized by XRF. The prepared silica particles were characterized by XRD and FTIR. The XRF results showed that the silica content obtained at temperature 1000 ℃ for 4 hrs was highest (88.13 %). The peaks for quartz silica appeared at multiple angles for samples treated at 1000 ℃ as compared to samples treated at 600 ℃. Moreover, the crystallinity level of silica quartz obtained varied with different concentrations of sodium hydroxide used for silica extraction.

Mokhtar and Tajuddin [6] in **2016** prepared silica from the waste material of sugarcane bagasse ash. The method followed was precipitation. The bagasse was treated with NaOH solution for three hrs to obtain sodium silicate solution. Acid treatment was carried out with H_2SO_4 until a pH 2 was maintained and then NH_4OH was added to maintain a pH of 8.5. SEM characterization was done to determine the cross-sectional area of the membrane and distribution of sugarcane bagasse nano silica (SCBN).

Sahiron *et al.* [5] in **2017** extracted silica from sugarcane bagasse waste produced in sugar industries. Sugarcane bagasse (SCB) was heated at different temperatures of 600, 800 and 1000 ℃ for 2 hrs and 4 hrs, respectively. The ash was then washed using hydrochloric acid (HCl) and boiled with 3 M NaOH solution to synthesize silica. The ash was characterized using XRF. The results indicated that the maximum silica yield of 88.13 % was obtained by SCBA burnt at 1000 ℃ for 4 hrs.

Rovani *et al.* [7] in **2018** obtained high purity nano silica from sugarcane bagasse ash. The fusion process was performed at 550 ℃ for 1 hr, varying the proportion (w:w) of ash:NaOH (1:0.5, 1:1, 1:1.5 and 1:2) to obtain sodium silicate. SEM micrograph of the final product prepared in the proportion of ash:NaOH (1:2) exhibited silica nanoparticles in the range between 50 - 500 nm. FTIR analysis demonstrated the presence of three main bands at 798 and 450 cm^{-1} ascribed to the siloxane groups (Si-O-Si) symmetric stretching and at 1060 cm^{-1} attributed to the siloxane groups (Si–O–Si) asymmetric stretching, respectively. XRD analysis indicated a wide peak at $2\theta = 22°$, which is a characteristic of pure amorphous silica. It is a facile synthesis method to extract highly pure nano silica from sugarcane bagasse.

Sapawe *et al.* [8] in **2018** obtained green silica content from six different agro-food waste such as sugarcane bagasse, bamboo culm, bamboo leaf, corncob, banana leaf and, cigarette butt. These wastes were washed several times with water in order to separate out any impurities. These samples were further combusted at 650 ℃ for 3 hrs to generate ash. The as-prepared ash from different materials was converted to silica by sol-gel method. Silica was purified by alkali extraction using 1 M NaOH, followed by acid precipitation with 1 M H_2SO_4. Among all the samples, sugarcane bagasse ash was found to contain high amount of silica (92.5 %). The higher percentage of silica produced from sugarcane bagasse ash revealed its potential for further investigations.

Channoy *et al.* [9] in **2018** prepared silica by calcining sugarcane bagasse ash at 700 ℃ for 4 and 6 hrs, respectively. The alkaline extraction method using different concentrations of sodium hydroxide (NaOH) (1.5, 2 and 2.5 N) was followed to purify bagasse ash. The ash was refluxed with 2 N conc. H_2SO_4. The results revealed that the composition of silica after heat treatment at 700 ℃ for 6 hrs was 80.81 wt%. The XRD patterns of synthesized silica using 2.5 N sodium hydroxide confirmed the amorphous nature of silica. SEM micrographs revealed the spherical morphology of synthesized silica particles with average size 80-100 nm. Also, the particle size was found to vary with the concentration of NaOH used.

Wee *et al.* [10] in **2019** extracted silica from rice husk via acid-alkaline precipitation method. The as-synthesized silica precipitate was thermally treated at various temperatures within a range of 600 -1200 ℃ in order to obtain dried silica powder. The

best results were observed for silica calcined at 1200 ℃. FT-IR spectra showed peaks of Si-O-Si in all the prepared samples. XRD results revealed the transformation of amorphous silica into crystalline form with a rise in calcination temperature. FE-SEM results illustrated the agglomeration of synthesized silica nanoparticles. It was observed that with the increase in calcination temperature the shape of silica particles changed from irregular to spherical shape.

Azat *et al.* [11] in **2019** synthesized pure silica powder from the waste product of rice husk. For this purpose, the acid-treatment procedure was followed. Three different samples of rice husk - without any pre-treatment, pre-treatment with HCl and pre-treatment with citric acid were prepared. The optimum calcination temperature of 600 ℃ was obtained from the preliminary TGA results. XRD results confirmed the formation of amorphous silica in all the three samples. SEM micrographs of untreated rice husk sample showed a network structure. However, acid treatment of rice husk leads to the dissociation of the network structure and resulted in the formation of nano silica particles. FT-IR analysis was done to depict the chemical bonding of the samples. XRF analysis showed that HCl pre-treatment method produced silica particles with maximum purity of 99.66 %. However, citric acid pre-treatment method also produced silica particles with a high purity of 98.67 %. The results indicated that citric acid pre-treatment method is an economic and environment friendly method to synthesize pure silica particles.

Adebisi *et al.* [12] in **2019** developed silica particles from the agricultural waste of maize stalk. Nano-silica particles were prepared via sol-gel technique. EDX analysis indicated the presence of higher silica content in acid treated sample than in untreated sample. The morphological properties revealed a lower degree of agglomeration in acid-treated sample in comparison to the untreated sample. XRD spectra showed the formation of amorphous silica. The amorphous silica was annealed at 1000 ℃ which resulted in the generation of crystalline phase named cristobalite. Short-ranged silica particles were successfully obtained with a particle size less than 30 nm.

Nataranjan *et al.* [13] in **2019** derived silica using sugarcane bagasse ash (SBA) to finally produce hydrophobic coatings on tiles. The silica was extracted via calcination and acid-treatment method. The thermal treatment was carried out in the temperature range 400-800 ℃. FE-SEM images showed rectangular morphology of SBA-500 ℃ while

spherical morphology was observed for SBA-750 ℃. EDS spectra indicated higher silica content in SBA-750 ℃ than in SBA-500 ℃. Further, the silica content was determined by XRF analysis. The silica content in SBA-500 ℃ and SBA-750 ℃ was found to be 88 % and 94 %, respectively. SBA coated tiles were successfully developed with high hydrophobicity which is due to the rough surface of SBA.

2.2. Literature survey of $CaCO_3$ and CaO from eggshells

Witoon [14] in **2011** extracted calcium carbonate from waste eggshells. The eggshells were first rinsed with deionized water (D.I.) and crushed into small particles. The prepared samples were heated at 900 ℃ for an hour in nitrogen atmosphere in order to remove carbon dioxide. The crystal structure of the developed samples was illustrated via XRD. The amount of calcined eggshell ($CaCO_3$)was determined from TGA analysis. The BET analysis was done to find out the surface area and porous volume.

Tangboriboon *et al.* [15] in **2012** used duck eggshells to extract calcium oxide using a simple method. The collected samples were calcined at temperatures varied from 300 to 900 ℃ for different time durations. The highest yield of calcium oxide was obtained at calcination conditions of 900 ℃ for 1 hr. Also, the purity of 99.06 % was obtained. The heat treatment given at 900 ℃ completely converted calcium carbonate ($CaCO_3$) into the calcium oxide (CaO). TEM images revealed a nearly uniform distribution of calcium oxide particles. The white calcium oxide powder prepared was highly porous and exhibited a narrow particle size distribution. The obtained yield as determined from STA analysis was 53.53 %.

Goloshchapov *et al.* [16] in **2013** used eggshells as a biological source for the synthesis of Hydroxyapatite (HAP). Firstly, the eggshells were thoroughly washed with distilled water and then annealed for 2 hrs at 900 ℃ to extract CaO from $CaCO_3$. The eggshells were found to comprise 95 % $CaCO_3$ and some other organic components that were burnt during annealing. The calcination process transformed $CaCO_3$ into CaO with 1 % impurity.

Correia *et al.* [17] in **2014** utilized egg and crab shells to derive calcium oxide. Calcium carbonate was partially modified into CaO after calcination at 900 ℃ for 2 hrs. The catalytic performance of as-prepared CaO powder in the transesterification process

was analyzed. The generation of little particles of calcium carbonate as well as calcium oxide after calcination accounted for this catalyst behavior.

Ummartyotin and Tangnorawich [18] in **2015** obtained calcium oxide from chicken eggshells. Eggshell waste was calcined at different temperatures ranging from 700 to 1000 ℃ for 3 hrs to extract calcium oxide. The SEM micrographs presented an irregular morphology with a varying particle size distribution. The extracted calcium oxide was used as a calcium precursor for the synthesis of hydroxyapatite.

Chraibi *et al.* [19] in **2016** efficiently prepared calcium oxide from calcining eggshells (CES). Preliminarily, the eggshells were thoroughly rinsed with water and dried at 60 ℃. The dried eggshells were sieved with a sieve of size 425 μm. The obtained powder was given thermal treatment at several temperatures 200, 400, 600, 800 and 1000 ℃, respectively. The calcinated eggshells were further used to explore the adsorption of phenol. The chemical composition of the obtained adsorbs was also examined.

Jirimali *et al.* [20] in **2017** developed calcium oxide from waste eggshells and used it to prepare hydroxyapatite. Primarily, the thermal treatment method was adopted for the formation of (CaO) calcium oxide. The waste eggshells were investigated by FTIR, XRD and SEM analysis. The SEM images demonstrated that the macro-porous structure of extracted calcium oxide. Moreover, hydroxyapatite biomaterial exhibited a crystalline form. Also, the particles formed were nanoscale at around 50-100 nm dimensions.

Wong and Ang [21] in **2018** derived calcium oxide from eggshells. The thermal treatment was given to eggshells using various calcination conditions such as temperature and time. The eggshells (calcium carbonate) which underwent calcination under 1000 ℃ were completely transformed into calcium oxide. The XRD analysis confirmed the crystallinity of the prepared samples. The catalytic activity of both the pure calcined CaO and calcined eggshell derived catalyst was comparable. The biodiesel formation was studied by gas chromatography-mass spectrometry (GC-MS).

Andherson *et al.* [22] in **2018** obtained calcium oxide from chicken egg shells and cacao pod wastes. The chicken eggshell powder was heated at four temperatures ranging from 600 to 900 ℃ for 6 hrs. The as-synthesized samples were characterized by XRD, FTIR and, SEM, respectively. The sharp peaks of the XRD spectra indicated the crystalline nature of the extracted CaO. The $CaCO_3$ phases appeared at $2\theta = 29.4^{o}$ and 47.3^{o} and

$Ca(OH)_2$ phases occurred at $2\theta = 28.6^o$, 34.2^o, 47.2^o and, 50.9^o. The most dominant phase CaO was obtained at thermal conditions of 900 ℃. FTIR analysis of chicken eggshells indicated the presence of OH group at peaks around 3639.06 - 3760.21 cm^{-1}.

Ummartyotin and Manuspiya [23] in **2018** extracted calcium oxide from waste egg shells and eventually prepared hydroxyapatite. The eggshells were calcined at 700, 800, 900 and 1000 ℃ for 2 hrs, respectively to synthesize calcium oxide. The morphology of the calcium oxide investigated by SEM analysis at higher magnification revealed the presence of rod-like particles. CO_2 evaporation during calcination resulted in the formation of pores.

Vera *et al.* [24] in **2018** synthesized calcium oxide (lime) from eggshells. Eggshells were washed with distilled water to remove any last traces of adhering impurities. Eggshells were rinsed using refined water, ground and calcined at different temperatures 600, 800, and 1000 ℃ for 1 hr, respectively. The thermal treatment caused surface evaporation of CO_2 from eggshells ($CaCO_3$) and finally, calcium oxide (CaO) was obtained as the end product. The experimental conditions of calcination temperature and time were optimized by performing TGA, FTIR and other qualitative tests.

Kavitha *et al.* [25] in **2019** obtained calcium oxide from eggshell waste via adopting calcination procedure. Eggshell derived calcium oxide was further utilized in the generation of biodiesel due to its catalytic activity. Several washings of the eggshells were done with lukewarm water to separate out any adhering thin membranes. The dried eggshells were ground and finally heat treatment was carried out at 800 ℃ for three hrs. The calcination treatment transformed $CaCO_3$ into CaO. The crystallite size of the calcium oxide particles was in the range 16-22 nm. Also, FT-IR analysis was done to determine the functional groups present in both the uncalcined and calcined eggshell samples. SEM images of the calcined eggshell sample revealed a highly porous structure.

Habte *et al.* [26] in **2019** extracted calcium oxide from waste eggshells via sol-gel technique. The crystallite size was found to be 24.51 nm. SEM images revealed spherical morphology of the synthesized CaO particles. The size of the synthesized particles was in the range 50-198 nm.

Kara *et al.* [27] in **2019** synthesized calcium oxide from chicken eggshells by simple thermal treatment. The as-obtained calcium oxide was used in the catalytic activity

for biodiesel production. The heat treatment was performed at 850 ℃ for 2 hrs in order to convert $CaCO_3$ (eggshell) into CaO. TGA analysis indicated maximum weight loss in the range 600-800 ℃. XRD and FT-IR analysis confirmed the formation of pure CaO in amorphous form. EDS spectra showed that the major component of calcined eggshell was calcium with a content of 98.21 %. The morphology of the as-prepared CaO showed a highly porous structure.

Rahman *et al.* [28] in **2019** derived calcium oxide from waste chicken eggshells via thermal treatment. A number of washings of eggshells were performed with tap and distilled water to remove adhering dust and other impurities. Washed eggshells were dried and crushed to form a fine powder. Then, the eggshells were subjected to thermal treatment at a temperature of 900 ℃ for a time duration of 4 hrs in order to obtain calcium oxide. XRD and FT-IR results assured the development of CaO phase. TGA results indicated major weight loss in the temperature range 650-750 ℃. This inferred that complete decomposition of $CaCO_3$ into CaO along with the release of CO_2 occurred at 750 ℃. SEM images of calcined eggshell showed irregular rod and dumbbell-shaped particles. The as-synthesized calcium oxide was used as a catalyst in the synthesis process of biodiesel.

2.3. Literature survey of calcium silicates

Nagabhushana *et al.* [29] in **2011** synthesized a progression of $CaSiO_3:Eu^{3+}$ (1–5 mol%) phosphors via combustion technique. The properties of phosphors were determined by XRD, FTIR, SEM and optical spectroscopy. The XRD diffractograms depicted the monoclinic structure of $CaSiO_3$ prepared at 900 ℃. The SEM micrographs revealed mostly angular and irregular shaped crystallites. The concentration quenching was observed for 4 mol% concentration of Eu^{3+}.

Qian *et al.* [30] in **2011** synthesized red light emitting $Ca_3Si_2O_7:Eu^{2+}$ phosphors by adopting solid-state reaction procedure. The as-developed samples showed a wide red band centered at wavelength 603 nm. The evaluated coordinates of emission color were (0.550, 0.438). Quenching was found to occur at 0.01 mol % concentration of Eu^{2+}. The as-synthesized phosphors were proved to be efficient red light emitting candidates.

Zhang *et al.* [31] in **2012** prepared $Ca_{3-x}Si_2O_7: xDy^{3+}$ (x = 0.03, 0.05, 0.07, 0.10) phosphors by varying concentration of Dy^{3+} ions. XRD pattern revealed that the host lattice structure remains unchanged for dopant concentration less than 0.10. SEM micrographs

showed aggregation of particles with irregular morphology. EDX analysis illustrated that the samples comprised of calcium, silicon, oxygen and, Dysprosium elements. The photoluminescence spectra at the excitation wavelength of 350 nm showed Dy^{3+} transitions of $^4F_{9/2} \rightarrow {}^6H_{15/2}$ and $^4F_{9/2} \rightarrow {}^6H_{13/2}$ attributed to blue and yellow emission color, respectively. The observed color coordinates of synthesized samples were observed to lie in the white light region.

Mao *et al.* [32] in **2012** synthesized tricolor emitting $Ca_3Si_2O_7$ phosphors doped with three lanthanides, Ln= Ce^{3+}, Eu^{2+}, Tb^{3+}. The PL spectra, characteristics of thermal quenching and illumination applications were worked upon. These phosphor materials activated with Ce^{3+}, Eu^{2+} and, Tb^{3+} ions produced blue, red, and green (three-basal-color) emission color, respectively. Phosphors doped with Ce^{3+} and Tb^{3+} showed better thermal quenching property in comparison to that of Eu^{2+} doped phosphors. CCT and CRI values of 6000 K and 87 were obtained.

Ju *et al.* [33] in **2013** synthesized $Ca_3Si_2O_7$:Ce^{3+}, Eu^{2+} phosphors by adopting solid-state technique. The occurrence of peaks at 450 nm and 610 nm correspond to Ce^{3+} and Eu^{2+} transitions, respectively. The color of emission was highly dependant on the Eu^{2+}/Ce^{3+} ratio. The emission color varied from blue to white and ultimately to orange with the varying ratio of Eu^{2+}/Ce^{3+}. The luminescence results revealed that the transfer of energy transmission from Ce^{3+} ion to Eu^{2+}ion was due to quadrupole-quadrupole interactions. The results revealed the use developed phosphors with tunable emission for the manufacturing of near-UV white LEDs.

Baran *et al.* [34] in **2013** synthesized β phased Ca_2SiO_4 activated by Eu^{2+} and Eu^{3+} dopant ions. The samples were prepared by solid-state technique. The three samples of Ca_2SiO_4:Eu^{2+}, Ca_2SiO_4:Eu^{3+} and Ca_2SiO_4:Eu^{2+}, Eu^{3+} samples were characterized by various techniques. The PL emission spectra of the Ca_2SiO_4:Eu^{2+}, Eu^{3+} sample revealed a combination of emission corresponding to Eu^{2+} and Eu^{3+} ions. The results confirmed the potential of dicalcium silicate (Ca_2SiO_4 or Ca_2S) as a suitable host material for luminescent lanthanide ions.

Mao *et al.* [35] in **2014** synthesized tricolor emitting lanthanide ion doped Ca_2SiO_4 phosphors by following the usual procedure of solid-state reactions. The prepared phosphors $Ca_{2(1-x)}SiO_4$:xCe^{3+},xLi^{+} blue, Ca_{2-x} SiO_4:xEu^{2+} green, and $Ca_{2(1-x)}SiO_4$:xSm^{3+},x

Li^+ (x = 0.005, 0.01, 0.02, 0.03 and 0.04 mol) were analyzed by techniques. β-Ca_2SiO_4 phase with a monoclinic structure was dominant. The photoluminescence of pure Ca_2SiO_4 host under UV excitation showed no luminescence because of the absence of dopants. The dopants acted as the emission centers in luminescent materials. The emission colors observed were blue, green and red for cerium, europium and, samarium doped phosphors, respectively.

Huang *et al.* [36] in **2014** developed $Ca_3Si_2O_7:Eu^{2+}$ phosphors with intense orange-yellow emission color. The XRD analysis using synchrotron radiation depicted monoclinic crystal structure of as-prepared phosphors. A broad yellow band centered at wavelength 603 nm was observed in PL spectra. 0.015 mol was the obtained optimum concentration of Eu^{2+} ion in the $Ca_3Si_2O_7:Eu^{2+}$ sample. CCT values were in the range of 1924 - 4992 K. The evaluated CIE color coordinates fell in between yellowish-orange to purplish red color. The results confirmed that the obtained phosphor finds application in white LED's.

Barve *et al.* [37] in **2015** synthesized Eu^{3+} doped calcium silicate $CaSiO_3:Eu^{3+}$ via co-precipitation route. The calculations of Judd–Ofelt parameters were done with the help of PL emission spectra of different Eu ion concentration. It was observed that the europium transition $^5D_0$ - $^7F_2$ was remarkably sensitive. The lifetime decay patterns were recorded for various Eu^{3+} concentrations. The obtained quantum efficiency was estimated to be 62 % while the lifetime of fluorescence was observed to be 2.9 msec.

Venkataravanappa *et al.* [38] in **2016** synthesized single-phased Ca_2SiO_4 nanoscale phosphors. The dopant ion Eu^{3+} concentration was varied from 1-5 mol %. The PL spectra revealed that $Ca_2SiO_4:Eu^{3+}$ phosphors exhibited powerful red color emission at a wavelength of 613 nm assigned to $^5D_0 \rightarrow {}^7F_2$ which is the transition of Eu^{3+}. Concentration quenching process was explained on the context of the transfer of energy of dopant, coupling of electron and phonon and interaction between the dopant ions. In addition, Judd–Ofelt (J–O) analysis and other properties of radiation were reported from emission spectra.

Zhang *et al.* [39] in **2017** developed Eu^{3+} doped calcium silicate. The sample showed red color emission at a wavelength of 612 nm. The synthesized product had a particle size of 100 nm and a huge surface area. The product prepared was also highly

biocompatible and exhibited excellent drug delivery characteristics. Hence, the as-obtained spherical composites find numerous biomedical applications such as drug delivery.

Woo *et al.* [40] in **2017** successfully developed Ca_2SiO_4 doped with Eu^{2+} ions. Silica was extracted from propylene glycol modified silane (PGMS). The differently aged PGMS used for synthesizing Eu^{2+} doped Ca_2SiO_4 phosphors greatly affected the emission color. The obtained results confirmed the color-tunable ability of the developed phosphors. Therefore, the studies indicated that the as-developed phosphors are expected to be efficient red light emitting candidates for economical use in the lighting industry.

Singh *et al.* [41] in **2017** synthesized Eu^{3+} activated $MSiO_3$ nanoscale phosphors via sol-gel method carried out at 950 ℃. Here, M stands for Ca, Mg, Sr, Ba. The samples were further reheated at 1050 and 1150 ℃ for 1 hr, respectively. The crystallinity of as-synthesized silicate phosphors was illustrated by the diffraction pattern. The results revealed that the synthesized powders existed in a single phase. The prepared $CaSiO_3$ exhibited monoclinic crystal structure. CIE color coordinates were obtained in the red domain. The structure and type of bonding existing in the prepared phosphors were determined by FTIR studies. TEM results confirmed the formation of nano-sized particles phosphor materials.

Devi *et al.* [42] in **2017** synthesized trivalent lanthanide ion dysprosium (Dy^{3+}) activated Ca_2SiO_4 phosphors through solid-state reaction method. Silica was extracted from rice husk agricultural waste. The synthesized Ca_2SiO_4 powders exhibited monoclinic crystalline structure. The SEM micrographs indicated irregular morphology. The effect of changing concentration of dopant ion was also studied in detail. The developed phosphors showed yellow as well as blue emission color corresponding to different Dy^{3+} ion transitions. These results indicated that Ca_2SiO_4:Dy^{3+} phosphors can be used for practical applications in optoelectronic devices.

Ueda *et al.* [43] in **2017** prepared $Ca_3Si_2O_7$ (CSO) activated with Eu^{2+} along with co-doping. The photoluminescence spectra revealed persistent orange emission. The starting luminescence of CSO:Eu^{2+}-Sm^{3+} and CSO:Eu^{2+}-Tm^{3+} was 290 and 9300 times powerful, respectively than the CSO:Eu^{2+}. Finally, the persistent luminescence duration was around 50 min in the sample CSO:Eu^{2+}-Tm^{3+} at optimum Eu^{2+} and Tm^{3+} concentrations.

Devi and Jayasankar [44] in **2018** synthesized europium activated Ca_2SiO_4 phosphors via solid state technique. The starting materials were extracted from the agro-food waste material of eggshells and rice husk. Europium transitions of $^5D_0 \rightarrow {}^7F_J$ were observed in the emission spectra. The color coordinates were located in the red region for all dopant concentrations. The lifetimes were found in the range from 2.67 to 2.78 ms. These low-cost phosphors showed marvelous luminescence properties.

He *et al.* [45] in **2018** successfully synthesized $(Ba,Ca)_2SiO_4$ phosphors following solid-state technique. The Eu^{2+}-activated T-phase $(Ba,Ca)_2SiO_4$ phosphors had a firm structure with atom site splitting. Further, the photometric studies depicted outstanding thermal stability of the developed phosphors. All these results confirmed that the as-synthesized phosphors are suitable for use in many optoelectronic applications.

Verma *et al.* [46] in **2018** synthesized calcium silicate phosphors via combustion method. The synthesis was performed at an initial temperature of 700-800 ℃. Er^{3+} and Tb^{3+} were used as activators. EDX analysis was done to find the composition of the elements in the prepared phosphor. The PL spectra revealed that both the phosphors showed intense green emission in the range of 650-680 nm. In addition, the prepared phosphors showed better color stability. The results proved that both these compositions could be employed as an efficient green light emitting phosphors for the generation of white LEDs.

Ozturk and Karacaoglu [47] in **2018** produced M_2SiO_4 (M = Ca, Zn) activated with 1 mol % Eu^{3+} via solid-state reaction method. The samples were given thermal treatments at 1200 ℃ for 3 hrs under an open atmosphere. The crystallographic and phase properties were examined by XRD. The two phosphor systems were entirely similar in structure excluding that the Zn_2SiO_4 exhibited some ZnO secondary phases. The photometric studies for both phosphors reported the transitions of the Eu^{3+} ions.

Devi et al. [48] **in 2018** synthesized lanthanide ion samarium (Sm^{3+}) activated Ca_2SiO_4 sample by adopting the traditional method of solid-state reactions. The precursors used SiO_2 and CaO were derived from agro-food wastes of rice husk and chicken egg shells, respectively. The as-prepared phosphors exhibited profound reddish-orange emission at a wavelength of 600 nm corresponding to Sm^{3+} ion transition $^4G_{5/2} \rightarrow {}^6H_{7/2}$.

Kaur and **Singh** [49] in **2019** successfully synthesized larnite (Ca_2SiO_4) and rankinite ($Ca_3Si_2O_7$) from the agro-food wastes of rice husk and eggshells. Rice husk was

used as a source of SiO_2 while eggshells as CaO source. The calcium silicates were synthesized via solid-state method. The heating temperature was varied from 1000-1350 ℃ which lead to the evolution of different phases of calcium silicates. Pure Ca_2SiO_4 phase was formed at 1250 ℃ while the formation of single phase $Ca_3Si_2O_7$ required a high heating temperature of 1400 ℃. XRD analysis was performed in order to determine the various phases formed in the samples. At room temperature, monoclinic and orthorhombic phases were obtained in Ca_2SiO_4. However, single monoclinic phase was stabilized via double heat treatment. In addition, a mixture of three phases, Ca_2SiO_4, $Ca_3Si_2O_7$ and, $CaSiO_3$, was obtained at lower sintering temperatures.

Mangalagowri *et al.* [50] in **2019** synthesized Er^{3+} doped Ca_2SiO_4 green light emitting phosphors via sonochemical method. The Er^{3+} concentration was varied from 1-11 mol %. XRD diffraction peaks revealed the formation of monoclinic phase. The varying dopant concentration produced no significant change in the XRD pattern. SEM and TEM micrographs revealed the spherical morphology of as-synthesized particles. The optical band width of the as-synthesized phosphors was within 4.95-5.18 eV. Concentration quenching occurred at 5 mol % Er^{3+} ions concentration. The evaluated CIE coordinates were found to lie in the green region. The obtained CCT value was 4548 K. The results indicated the potential application of as-synthesized phosphors in the manufacturing of cool LEDs.

Lu *et al.* [51] in **2019** synthesized $Ca_2SiO_4:Eu^{3+}$ phosphors using commercially available chemical reagents via solid-state sintering method. Eu^{3+} concentration was varied from 0.01-1 at %. XRD diffraction peaks indicated the formation of γ and β- Ca_2SiO_4 phases. It was examined that increasing dopant ion concentration enhanced the formation of β- Ca_2SiO_4 phase. Also, with a rise in dopant concentration, the transition $^5D_0 \rightarrow {}^7F_2$ was found to intensify while the reduction of the intensity of $^5D_0 \rightarrow {}^7F_1$ transition was observed. The study revealed the potential utilization of Eu^{3+} for phase identification.

Verma *et al.* [52] in **2019** prepared a series of $CaSiO_3:xTb^{3+}$ (x = 1-10 mol %) phosphors by solution combustion method. XRD results showed that increasing Tb^{3+} concentration caused the phase conversion of $CaSiO_3$ to $Ca_3Si_2O_7$. The average size of the crystallite was 68.50 nm. The PL emission spectra revealed the green emission of as-synthesized phosphors attributed to Tb^{3+} ions corresponding to $^5D_4 \rightarrow {}^7F_5$ transition at 545

nm. The emission intensity was found to increase up to 7 mol % Tb^{3+} ions concentration. The activation energy of as-synthesized phosphors determined from the thermoluminescence study was 0.86 eV. These phosphors proved to be suitable green light emitting candidates in the formation of low-cost organic light emitting diodes (OLED's).

Based on the literature survey, the outcomes of different research papers including synthesis method, morphology, crystallite/particle size, emission and, excitation wavelengths are summarised in Table 2.1.

Table 2.1: Comparative literature survey of rare earth doped calcium silicate phosphors

S. No.	Compound	Synthesis method	Morphology	Size	PL excitation/ emission wavelength (nm)	Key findings
1.	$CaSiO_3:Eu^{3+}$ (1-5 mol%) [29]	Solution combustion method	Irregular shape	30-50 nm	254/ 581, 593, 614, 654, 724	i. Concentration quenching occurred at 4 mol% Eu^{3+}. ii. Monoclinic phase was obtained at 900 ℃.
2.	$Ca_{3-x}Si_2O_7:xEu$ (x = 0.002–0.03) [30]	Solid-state reaction method	-	-	345, 400, 460/ 570, 603, 630	i. Concentration quenching occured for x = 0.01.
3.	$Ca_{3-x}Si_2O_7:xDy^{3+}$ (x = 0.03, 0.05, 0.07, 0.10) [31]	Solid-state reaction method	Irregular	-	350/ 484, 574	i. Dy^{3+} substitution of Ca^{2+} did not change the structure of host for $x \leq 0.10$. ii. Concentration quenching occurred for x = 0.05.
4.	$Ca_3Si_2O_7:Ln$ ($Ln = Ce^{3+}, Eu^{2+}, Tb^{3+}$) (x = 0.002, 0.004, 0.006, 0.008, 0.01 and 0.012) [32]	Solid-state reaction method	-	-	For $Ca_{3-x}Si_2O_7:xEu$ 350/ 597 For $Ca_{3-x}Si_2O_7:xCe$ 350/ 415 For $Ca_{3-x}Si_2O_7:xTb$ 350/ 542	i. Better thermal quenching property of Ce^{3+} and Tb^{3+} was recorded in comparison with Eu. ii. CIE chromaticity coordinates (0.32, 0.30) with CCT of 6000 K and CRI of 87.
5.	$Ca_2SiO_4:Eu^{2+}$, $Ca_2SiO_4:Eu^{3+}$ and $Ca_2SiO_4:Eu^{2+}$, Eu^{3+} [33]	Solid-state reaction	-	-	For $Ca_2SiO_4:Eu^{3+}$ 320, 420, 440, 460/ 510, 600 For $Ca_2SiO_4:Eu^{2+}$ 320, 460/ 510, 602 For $Ca_2SiO_4:Eu^{2+}$, Eu^{3+} 260, 320/ 620, 510	i. The luminescence spectra of the $Ca_2SiO_4:Eu^{2+}$, Eu^{3+} system was independent of temperature from 18 K to ambient.
6.	$Ca_3Si_2O_7:Eu^{2+}$ [36]	Solid-state reaction	-	-	460/ 603	i. Concentration quenching occurred at Eu^{2+} concentration = 0.015.
7.	$CaSiO_3:Eu^{3+}$ (1-5 mol%) [37]	Co-precipitation method	-	-	394/ 611	i. The quantum efficiency was found to be 62% from the emission spectrum. ii. The fluorescence lifetime was found to be 2.9 msec. iii. Concentration quenching occurred at 5 mol%.
8.	$Ca_2SiO_4:Eu^{3+}$ (1-5 mol%) [38]	Chemical route	Needle- like	-	299, 320, 360, 381, 393 and 414/ 613	i. Concentration quenching occured at 4 mol%.
9.	$CaSiO_3:Eu^{3+}$ [39]	Chemical route	Uniform nanospheres	100 nm	262/ 612	i. Potential application as a drug carrier in bio-medical field.
10.	$Ca_2SiO_4:Eu^{2+}$ [40]	Sol-gel process	-	-	400, 450/ 630	i. Differently aged propylene glycol modified silane (PGMS) was used as silica source. ii. The luminescence characteristics of differently aged PGMS phosphors could be well tuned from reddish yellow to green.
11.	$MSiO_3$ (M = Mg, Ca, Sr and Ba) [41]	Sol-gel process	-	-	395/ 610-615	i. The transformation from β to α phase of $CaSiO_3$ took place at 1300 ℃.
12.	$Ca_2SiO_4:Dy^{3+}$ [42]	Solid-state reaction	Irregular	33 nm	351, 366, 387/ 573	i. The color coordinates obtained from emission spectra were found to fall within the white light zone.
13.	$Ca_3Si_2O_7$(CSO)Eu^{2+}, CSO:Eu^{3+}, CSO:Ce^{3+} and CSO: Eu^{2+}-Tm^{3+} [43]	Solid-state reaction	-	-	For CSO:Eu^{2+} and CSO:Eu^{2+}-Tm^{3+} 400/ 620 For CSO:Eu^{3+} 394/ 613	i. In CSO:Eu^{2+} (0.1%)-Tm^{3+}(0.5%), the persistent luminescence duration on 0.32 mcd/m^2 reached 50 min.

					For CSO:Ce^{3+} 300/ 380, 500	
14.	Ca_2SiO_4:xEu^{3+} (x = 0.01-0.4%) [44]	Solid-state reaction	Non-uniform, irregular	35.4 nm	394/ 703	i. The effective emission CIE chromaticity coordinates were in deep red region.
15.	$(Ba,Ca)_2SiO_4$:Eu^{2+} [45]	Solid-state reaction	-	-	340/ 460-500	i. The luminescent thermal stability decreased with increase in Ca^{2+} content.
16.	$CaSiO_3$:Er^{3+} and $CaSiO_3$:Tb^{3+} [46]	Combustion method	Non-uniform	68.5 nm	For $CaSiO_3$:Er^{3+} 440/ 640-720 For $CaSiO_3$:Tb^{3+} 370/ 418, 438, 460, 493, 550, 590, 625	i. The morphology revealed that $CaSiO_3$:Tb^{3+} was more amorphous than $CaSiO_3$:Er^{3+}.
17.	M_2SiO_4 (M = Ca, Zn):1mol% Eu^{3+} [47]	Solid-state reaction	-	-	282/ 615	i. No XRD peak shifting was observed with incorporation of Eu^{3+} ions.
18.	Ca_2SiO_4:Sm^{3+} [48]	Solid-state reaction	-	-	404/ 600	i. The decay curves exhibited single exponential at lower concentration and turned into non-exponential at higher concentrations accompanied by shortening in lifetime. ii. CIE co-ordinates were in orange-reddish region.
19.	Ca_2SiO_4:Er^{3+} [50]	Sono-chemical	Spherical	-	402/ 517, 551, 613, 662	i. Concentration quenching was observed at 5 mol % Er^{3+} concentration. ii. CCT value was found to be 4548 K.
20.	$CaSiO_3$:Tb^{3+} [52]	Solution combustion	-	68.5 nm	257/ 545	i. The increasing Tb^{3+} concentration transformed $CaSiO_3$ into $Ca_3Si_2O_7$. ii. The optimum Tb^{3+} concentration was 7 mol %.

REFERENCES

[1] Nazriati, H. Setyawan, S. Winardi, Synthesis of silica aerogel from bagasse ash by ambient pressure drying, AIP Conf. Proc. 1415 (2011) 114–116.

[2] R. Yuvakkumar, V. Elango, V. Rajendran, N. Kannan, High-purity nano silica powder from rice husk using a simple chemical method, J. Exp. Nanosci. 9 (2014) 272–281.

[3] A. M. Usman, A. Raji, N. H. Waziri, M. A. Hassan, A Study on Silica and Alumina Potential of the Savannah Bagasse Ash , IOSR J. Mech. Civ. Eng. 11 (2014) 48–52.

[4] V. Vaibhav, U. Vijayalakshmi, S.M. Roopan, Agricultural waste as a source for the production of silica nanoparticles, Spectrochim. Acta - Part A Mol. Biomol. Spectrosc. 139 (2015) 515–520.

[5] N. Rahmat, Characterization of Sodium Silicate Derived From Sugarcane Bagasse Ash, Malaysian J. Anal. Sci. 21 (2017) 512–517.

[6] H. Mokhtar, R.M. Tajuddin, The Effect of Nanosilica Extracted from Sugarcane Bagasse on Formulation of Flat Sheet Nanofiltration Membrane, Int. J. Chem. Eng. Appl. 7 (2016) 323–326.

[7] S. Rovani, P. Corio, D.A. Fungaro, Sugarcane Biomass Ash as a Renewable Source of Nanosilica Sugarcane Biomass Ash as a Renewable Source of Nanosilica, : 46th World Chemistry Congress, (2017).

[8] N. Sapawe, N. Surayah Osman, M. Zulkhairi Zakaria, S. Amirul Shahab Syed Mohamad Fikry, M. Amir Mat Aris, Synthesis of green silica from agricultural waste by sol-gel method, Mater. Today Proc. 5 (2018) 21861–21866.

[9] C. Channoy, S. Maneewan, C. Punlek, S. Chirarattananon, Preparation and Characterization of Silica Gel from Bagasse Ash, Adv. Mater. Res. 1145 (2018) 44–48.

[10] N. Nur, A. Nik, A. Samsuri, N. Latif, Synthesis of silica from rice husk using acid pretreatment and its characterization, Materials Characterization using X-rays and Related Techniques, 020068 (2019) 6–11.

[11] S. Azat, A. V Korobeinyk, K. Moustakas, V.J. Inglezakis, Sustainable production of pure silica from rice husk waste in Kazakhstan, J. Clean. Prod. (2019).

[12] A.I. Journal, J.A. Adebisi, J.O. Agunsoye, S. Adekunle, M. Haris, M.M. Ramakokovhu, M. Olawale, Green production of silica nanoparticles from maize stalk, Part. Sci. Technol. 0 (2019) 1–9.

[13] S. Natarajan, S.T. Subramaniyam, V. Kumaravel, applied sciences Fabrication of Hydrophobic Coatings Using Sugarcane Bagasse Waste Ash as Silica Source, (2019), 9(1),190.

[14] T. Witoon, Characterization of calcium oxide derived from waste eggshell and its application as CO_2 sorbent, Ceram. Int. 37 (2011) 3291–3298.

[15] N. Tangboriboon, R. Kunanuruksapong, A. Sirivat, R. Kunanuruksapong, A. Sirivat, Preparation and properties of calcium oxide from eggshells via calcination, Mater. Sci. Pol. 30 (2012) 313–322.

[16] D.L. Goloshchapov, V.M. Kashkarov, N.A. Rumyantseva, P. V. Seredin, A.S. Lenshin, B.L. Agapov, E.P. Domashevskaya, Synthesis of nanocrystalline hydroxyapatite by precipitation using hen's eggshell, Ceram. Int. 39 (2013) 4539–

4549.
[17] L.M. Correia, R.M.A. Saboya, N. de Sousa Campelo, J.A. Cecilia, E. Rodríguez-Castellón, C.L. Cavalcante, R.S. Vieira, Characterization of calcium oxide catalysts from natural sources and their application in the transesterification of sunflower oil, Bioresour. Technol. 151 (2014) 207–213.
[18] S. Ummartyotin, B. Tangnorawich, Utilization of eggshell waste as raw material for synthesis of hydroxyapatite, Colloid Polym. Sci. 293 (2015) 2477–2483.
[19] S. Chraibi, H. Moussout, F. Boukhlifi, H. Ahlafi, M. Alami, Utilization of Calcined Eggshell Waste as an Adsorbent for the Removal of Phenol from Aqueous Solution, J. Encapsulation Adsorpt. Sci. 06 (2016) 132–146.
[20] H.D. Jirimali, B.C. Chaudhari, J.C. Khanderay, S.A. Joshi, V. Singh, A.M. Patil, V. V. Gite, Waste Eggshell-Derived Calcium Oxide and Nanohydroxyapatite Biomaterials for the Preparation of LLDPE Polymer Nanocomposite and Their Thermomechanical Study, Polym. - Plast. Technol. Eng. 57 (2018) 804–811.
[21] Y.C. Wong, R.X. Ang, O. Access, Study of calcined eggshell as potential catalyst for biodiesel formation using used cooking oil, Open Chemistry 16 (2018) 1166–1175.
[22] T. Andherson, D. Rachmat, D.D. Risanti, Potential use of chicken egg shells and cacao pod husk as catalyst for biodiesel production, AIP Conf. Proc. 1945 (2018) 020058 -1–020058-8.
[23] S. Ummartyotin, H. Manuspiya, A critical review of eggshell waste: An effective source of hydroxyapatite as photocatalyst, J. Met. Mater. Miner. 28 (2018) 124–13.
[24] F. Luna Vera, M. Guancha Chalapud, I. Castillo Viveros, E.A. Vasquez Medina, From Eggshells to Quicklime: Using Carbonate Cycle as an Integrating Concept to Introduce Students to Materials Analysis by TGA and FTIR, J. Chem. Educ. 95 (2018) 625–630.
[25] V. Kavitha, V. Geetha, P.J. Jacqueline, SC, Production of Biodiesel from Dairy Wasre Scum using Eggshell Waste, Process Saf. Environ. Prot. (2019).
[26] L. Habte, N. Shiferaw, D. Mulatu, T. Thenepalli, Synthesis of Nano-Calcium Oxide from Waste Eggshell by Sol-Gel Method, (n.d.) 1–10.
[27] K. Kara, F. Ouanji, M. El Mahi, E.M. Lotfi, M. Kacimi, Z. Mahfoud, Biodiesel synthesis from vegetable oil using eggshell waste as a heterogeneous catalyst, Biofuels. 0 (2019) 1–7.
[28] W.U. Rahman, A. Fatima, A.H. Anwer, M. Athar, M.Z. Khan, N.A. Khan, G. Halder, SC, Biodiesel synthesis from eucalyptus oil utilizing waste eggshell derived calcium based metal oxide catalyst, Process Saf. Environ. Prot. 122 (2019) 313-319.
[29] H. Nagabhushana, B.M. Nagabhushana, M. Madesh Kumar, Chikkahanumantharayappa, K.V.R. Murthy, C. Shivakumara, R.P.S. Chakradhar, Synthesis, characterization and photoluminescence properties of $CaSiO_3:Eu^{3+}$ red phosphor, Spectrochim. Acta - Part A Mol. Biomol. Spectrosc. 78 (2011) 64–69.
[30] F. Qian, R. Fu, S. Agathopoulos, X. Gu, X. Song, Synthesis and luminescence properties of a broad-band red phosphor $Ca_3Si_2O_7:Eu^{2+}$ for warm white light-emitting diodes, J. Lumin. 132 (2012) 71–75.
[31] X. Zhang, Z. Lu, F. Meng, L. Hu, X. Xu, J. Lin, C. Tang, Luminescence properties of $Ca_3Si_2O_7$: Dy^{3+} phosphor for white light-emitting diodes, Mater. Lett. 79 (2012) 292–295.

[32] Z.Y. Mao, Y.C. Zhu, L. Gan, Y. Zeng, F.F. Xu, Y. Wang, H. Tian, J. Li, D.J. Wang, Tricolor emission $Ca_3Si_2O_7$:Ln (Ln = Ce, Tb, Eu) phosphors for near-UV white light-emitting-diode, J. Lumin. 134 (2013) 148–153.

[33] H. Ju, L. Wang, B. Wang, Y. Ma, H. Wang, S. Chen, X. Tao, Single-phased emission-tunable $Ca_3Si_2O_7:Ce^{3+}$, Eu^{2+} phosphors for white light-emitting diodes, Ceram. Int. 39 (2013) 8001–8005.

[34] A. Baran, J. Barzowska, M. Grinberg, S. Mahlik, K. Szczodrowski, Y. Zorenko, Binding energies of Eu^{2+} and Eu^{3+} ions in β-Ca_2SiO_4 doped with europium, Opt. Mater. (Amst). 35 (2013) 2107–2114.

[35] Z.Y. Mao, Y.C. Zhu, Y. Wang, L. Gan, Ca_2SiO_4:Ln (Ln = Ce^{3+}, Eu^{2+}, Sm^{3+}) tricolor emission phosphors and their application for near-UV white light-emitting diode, J. Mater. Sci. 49 (2014) 4439–4444.

[36] C.H. Huang, W.R. Liu, T.S. Chan, Y.T. Lai, Orangish-yellow-emitting $Ca_3Si_2O_7:Eu^{2+}$ phosphor for application in blue-light based warm-white LEDs, Dalt. Trans. 43 (2014) 7917–7923.

[37] R.A. Barve, N. Suriyamurthy, B.S. Panigrahi, B. Venkatraman, Optical properties and Judd–Ofelt analysis of Eu^{3+} activated calcium silicate, Phys. B Condens. Matter. 475 (2015) 156–161.

[38] M. Venkataravanappa, H. Nagabhushana, G.P. Darshan, B. Daruka Prasad, G.R. Vijayakumar, H.B. Premkumar, Udayabhanu, Novel EGCG assisted ultrasound synthesis of self-assembled $Ca_2SiO_4:Eu^{3+}$ hierarchical superstructures: Photometric characteristics and LED applications, Ultrason. Sonochem. 33 (2016) 226–239.

[39] C. Zhang, W. Wei, J. Zhang, Y. Li, G. Zhou, G. Jia, Uniform mesoporous $CaSiO_3:Eu^{3+}$ nanospheres: Template-directed synthesis, luminescence and sustained drug release properties, Dye. Pigment. 136 (2017) 427–433.

[40] H.J. Woo, S. Gandhi, M. Jayasimhadri, D.S. Shin, H.S. Lee, K. Jang, Engendering color tunable emission in calcium silicate based phosphors via ageing of silicate source, Sensors Actuators, B Chem. 241 (2017) 1106–1110.

[41] D. Singh, S. Sheoran, V. Tanwar, S. Bhagwan, Optical characteristics of Eu(III) doped $MSiO_3$ (M = Mg, Ca, Sr and Ba) nanomaterials for white light emitting applications, J. Mater. Sci. Mater. Electron. 28 (2017) 3243–3253.

[42] L.L. Devi, C. Basavapoornima, V. Venkatramu, P. Babu, C.K. Jayasankar, Synthesis of $Ca_2SiO_4:Dy^{3+}$ phosphors from agricultural waste for solid-state lighting applications, Ceram. Int. 43 (2017) 16622–16627.

[43] J. Ueda, R. Maki, S. Tanabe, Vacuum Referred Binding Energy (VRBE)-Guided Design of Orange Persistent $Ca_3Si_2O_7:Eu^{2+}$ Phosphors, Inorg. Chem. 56 (2017) 10353–10360.

[44] L.L. Devi, C.K. Jayasankar, Spectroscopic investigations on high efficiency deep red-emitting $Ca_2SiO_4:Eu^{3+}$ phosphors synthesized from agricultural waste, Ceram. Int. 44 (2018) 14063–14069.

[45] L. He, Z. Song, X. Jia, Z. Xia, Q. Liu, Consequence of Optimal Bonding on Disordered Structure and Improved Luminescence Properties in T-Phase $(Ba,Ca)_2SiO_4:Eu^{2+}$ Phosphor, Inorg. Chem. 57 (2018) 4146–4154.

[46] S.Verma, A. Mishra, M. Bhuie, N.K. Singh, Comparative analysis of luminescence Property of Tb^{3+} and Er^{3+} Activated Calcium Silicate Phosphor, International Journal of Computer Science and Engineering, 6 (2018) 108-114.

[47] E. Ozturk, E. Karacaoglu, The Effect of Ligand-To-Eu^{3+} Charge-Transfer Transitions (Lmct) on the Photoluminescence Intensity of M_2SiO_4: Eu^{3+}(M = Ca, Zn) Type Phosphors, Mater. Sci. Pol. 36 (2018) 509–513.

[48] L.L. Devi, C. Basavapoornima, V. Venkatramu, C.K. Jayasankar, J. Kaewkhao, W. Lertlop, Structural and luminescence properties of Sm^{3+}- doped Ca_2SiO_4 phosphors from agricultural waste, Mater. Today Proc. 5 (2018) 15081–15085.

[49] M. Kaur, K. Singh, Evolution of Ca_2SiO_4 and $Ca_3Si_2O_7$ Crystalline Phases Synthesized from Agro-Food Waste Ashes, National Conference on Recent Advances in Condensed Matter Physics, 020033 (2019) 1–5.

[50] M. Mangalagowri, R.B. Basavaraj, G.P. Darshan, M.S. Raju, Y. V Naik, D. Kavyashree, H.K. Inamdar, S.C. Sharma, H. Nagabhushana, Sonochemical synthesis of green emitting Ca_2SiO_4:Er^{3+} nanopowders : Promising applications in optical thermometry and radiation dosimeter, Opt. Mater. (Amst). 92 (2019) 125–135.

[51] X. Lu, S. Wang, S. Liu, P. Du, Z. Ye, X. Geng, X. Cheng, Phase Identification of γ and β-Ca_2SiO_4 via the Rear-Earth Fluorescence Probe, The Journal of Physical Chemistry C ., (2019) 1-26.

[52] O.P. Verma, S. Verma, M.R. Meshram, N.K. Singh, Luminescence and impedance analysis of $CaSiO_3$:Tb^{3+} nano phosphors material prepared by combustion method for OLED, International Journal of Computer Sciences and Engineering, 7 (2019) 34-39.

CHAPTER 3
GAPS IN STUDY

After peer-review of literature survey, it has been observed that multiple research studies have been carried out to synthesize rare-earth activated calcium silicate phosphors via different techniques. Most of these studies involve the synthesis of calcium silicates via commercially available precursors which is not cost-effective. Moreover, commercial synthesis process requires sophisticated reaction condition parameters and apparatus. These parameters are not suitable for large scale production.

In the quest of utilization of agro-food waste materials to get treasured products, many researchers have made attempts to fabricate phosphor materials. Devi et al. [1-3] synthesized Ca_2SiO_4:Eu, Dy, Sm phosphors using rice husk ash (silica source) and eggshell powder (CaO source). Punj and Singh [4] synthesized inherent blue-light emitting phosphors utilizing corn husk and sugarcane leaves ash (as silica source). These reports demonstrated the use of agro-food ashes as such for the fabrication of desired products. But, it is a well-known fact that such ashes don't consist of pure silica. There are also other metallic by-products present along with the silica content. These elements also interfere in the structural, optical and luminescent properties. Moreover, the silica content also depends on the type of soil, crop and harvesting conditions. Thus, it is not feasible to use these agro ashes as such in the fabrication of materials. Further treatment is required to use these waste ash products for the fabrication of luminescent materials as phase purity is one of the essential requirements for intense and pure light emission.

REFERENCES

[1] L.L. Devi, C.K. Jayasankar, Spectroscopic investigations on high efficiency deep red-emitting $Ca_2SiO_4:Eu^{3+}$ phosphors synthesized from agricultural waste, Ceram. Int. 44 (2018) 14063–14069.

[2] L.L. Devi, C. Basavapoornima, V. Venkatramu, P. Babu, C.K. Jayasankar, Synthesis of $Ca_2SiO_4:Dy^{3+}$ phosphors from agricultural waste for solid-state lighting applications, Ceram. Int. 43 (2017) 16622–16627.

[3] L.L. Devi, C. Basavapoornima, V. Venkatramu, C.K. Jayasankar, J. Kaewkhao, W. Lertlop, Structural and luminescence properties of Sm^{3+}- doped Ca_2SiO_4 phosphors from agricultural waste, Mater. Today Proc. 5 (2018) 15081–15085.

[4] S. Punj, K. Singh, Blue-green light emitting inherent luminescent glasses synthesized from agro-food wastes, J. Mater. Sci. Mater. Electron. 30 (2019) 3871–3881.

CHAPTER 4
OBJECTIVES

In order to fill the gaps in the existing literature of Ca_2SiO_4, a simple, facile and novel route has been proposed in the present study. The primary objectives of this research work are as follows:

- To derive silica from sugarcane bagasse ash via acid-base precipitation technique.
- To extract calcium oxide from chicken eggshells employing calcination.
- To synthesize Eu-doped Ca_2SiO_4 phosphors via standard solid-state technique utilizing agro-food derived precursors.
- Characterization of synthesized materials by X-ray Diffraction (XRD), Scanning Electron Microscopy (SEM), Energy Dispersive Spectroscopy (EDS), UV/Visible Spectroscopy, Fourier Transform Infrared Spectroscopy (FT-IR) and Photoluminescence (PL) techniques.
- Calculation of several photometric parameters such as International Commission on Illumination (CIE) coordinates and Correlated Color Temperature (CCT) values from emission spectra.

CHAPTER-5
RESEARCH METHODOLOGY

5.1. Materials:

The precursors utilized for the facile synthesis of calcium silicates were extracted from the agricultural and food wastes. Silica (SiO_2) and calcium oxide (CaO) were used as starting materials. SiO_2 was extracted from sugarcane bagasse ash. Sugarcane bagasse was collected from sugarcane fields near Sirhind Road, Patiala, Panjab, India. CaO was extracted utilizing waste eggshells collected from Hostel -N canteen, TIET, Patiala. Europium oxide (Eu_2O_3) (*HiMedia*, purity 99.99%) was used as a dopant material. Sodium hydroxide pellets (NaOH) (*SDFC Ltd.*) and sulphuric acid (H_2SO_4) (*Loba Chemie Pvt. Ltd.*, purity 98%) were used for silica extraction. These reagents were analytically graded and were utilized as such without any refinement process.

5.2. Synthesis method:

i. Silica extraction (SiO_2) from sugarcane bagasse ash:

The pure silica was extracted from sugarcane bagasse ash via chemical treatment. The sugarcane bagasse collected from fields was given washing treatments to separate out any adhere dust particles. The as-washed sugarcane bagasse was subjected to drying and then burnt in an open atmosphere to form ash powder. The ash was calcined at 600 ℃ for a time duration of four hrs in a programmable muffle furnace with a rate of heating of 3 ℃/min to remove volatile gases. A batch of 10 g ash sample was chemically treated with 100 ml volume of 2 N sodium hydroxide solution under constant stirring at 80 ℃ for 2 hrs to obtain sodium silicate solution. The obtained solution was filtered with Whatsmann filter paper to remove carbonaceous and other metallic impurities. The resultant filtrate was titrated against 5 N sulphuric acid under constant stirring until pH range 5-6 to obtain gel-like silica. The gel obtained was aged for 24 hours. A number of washing treatments are performed with D.I. water to separate the last traces of salt impurities. The as-obtained gel was dried in an oven at 110 ℃ for 12 hrs. Silica powder was obtained after drying and crushing to small-scale particles. The extracted silica was amorphous in nature which was confirmed from the XRD results. The yield of silica was 70% through this chemical

treatment method. The chemical equations describing silica extraction can be represented as:

$$SiO_2 \text{ (bagasse ash)} + NaOH \rightarrow Na_2SiO_3 + H_2O \quad (1)$$

$$Na_2SiO_3 + H_2SO_4 \rightarrow SiO_2 + Na_2SO_4 + H_2O \quad (2)$$

ii. Calcium oxide (CaO) extraction from eggshells:

Waste eggshells were washed thoroughly many times with warm water to eliminate adhering impurities and membranes. The eggshells were heated in an oven at 70 ℃ for a total of 24 hours. Then, they were crushed manually to form a fine powder. In order to extract CaO, a batch of 10 g dried eggshell powder was calcinated at 950 ℃ for 2 hrs in a programmable muffle furnace. The furnace was maintained at 3 ºC/min. The obtained calcined powder was ground in mortar and pestle thoroughly. The yield of the obtained CaO was 95%. The chemical equation describing the calcium oxide extraction from eggshells can be represented as:

$$CaCO_3 \text{ (eggshells)} \xrightarrow{\Delta} CaO + CO_2 (\uparrow) \quad (3)$$

iii. Synthesis of Eu^{3+} doped and undoped Ca_2SiO_4 phosphors:

Pure and Eu^{3+} doped $Ca_{(2-x)}SiO_4:xEu^{3+}$ (x = 0.1-0.5 mol %) phosphors were developed by acquiring solid-state reaction technique. The amount of SiO_2 and CaO were precisely weighed stoichiometrically according to the chemical formula Ca_2SiO_4 and crushed in an agate mortar for about an hour. The ground samples were pre-heated at a temperature of 1250 ℃ for 6 hrs in muffle furnace maintained at 5 ℃/min. Then, the as-prepared powder was ground to form a homogeneous powder. The sample was again subjected to heat treatment in the muffle furnace at 1250 ℃ for 6 hrs to remove the intermediate phases obtained in the previous sample. The Eu-doped samples were also synthesized by following the above synthesis steps. In Eu-doped samples, Eu_2O_3 was taken in the stoichiometric ratio in addition to CaO and SiO_2 to synthesize $Ca_{(2-x)}SiO_4:xEu^{3+}$ phosphors. The as-prepared calcium silicate samples were ground well and subjected to further characterizations.

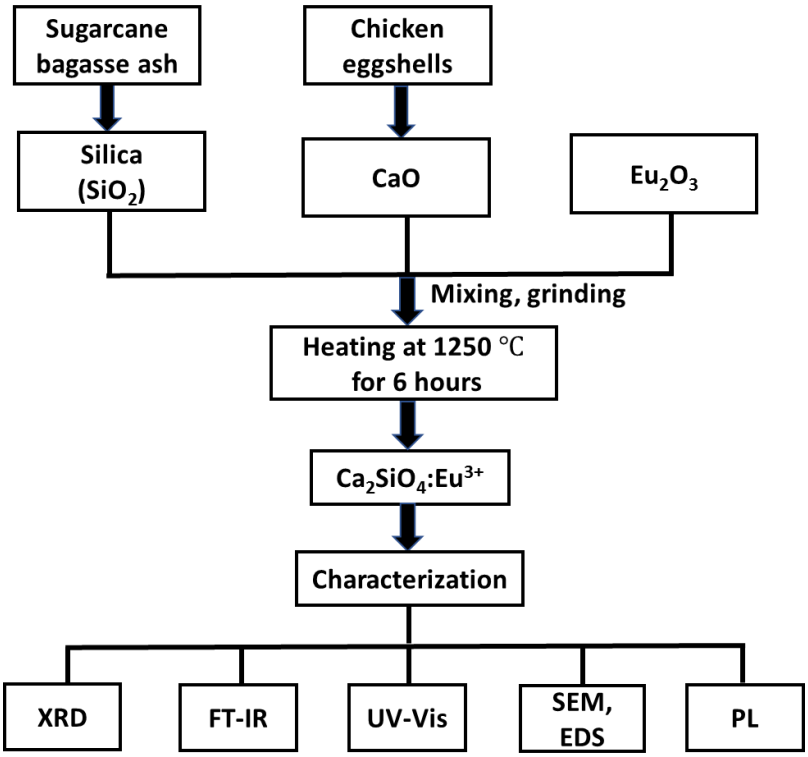

Figure 5.1: Schematic diagram of the synthesis method of calcium silicate phosphors

CHAPTER-6

RESULTS AND DISCUSSIONS

6.1. X-ray diffraction (XRD)

(i) X-ray analysis of sugarcane bagasse ash derived silica

Fig. 6.1 (a) represents the XRD pattern of sugarcane bagasse ash calcined at 600 ℃ for 4 hrs. The diffraction peaks reveal the presence of amorphous silica along with some organic impurities. The unwanted impurities are removed with acid treatment and base precipitation. For this purpose, sugarcane bagasse ash was treated with H_2SO_4 and NaOH alkali solution. Fig. 6.1 (b) represents the XRD pattern of silica gel having peaks of Na_2SO_4. The obtained XRD spectra ideally matched with standard International Centre for Diffraction Data (ICDD) card number: 01-086-080 representing peaks of Na_2SO_4. The chemically prepared silica gel was further washed with distilled water (D.I) to eliminate sodium sulfate present in the system. Fig. 6.1 (c) represents the XRD spectra of pure amorphous silica with a characteristic broad hump at $\sim 2\theta = 22.16^{o}$ [1]. The washing treatment accounted for the removal of all the peaks corresponding to the impure phases. The absence of any sharp peaks in the XRD spectra elucidates the amorphous nature of silica.

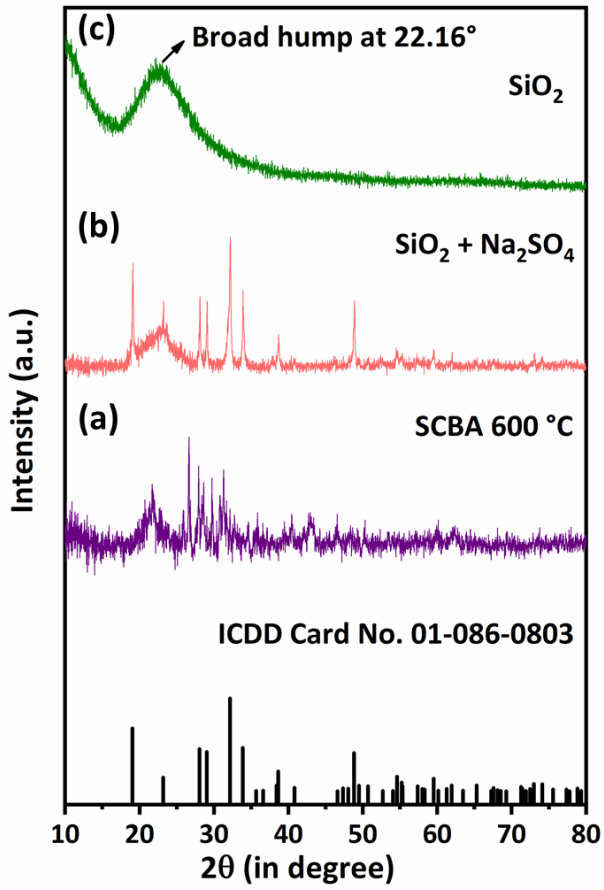

Figure 6.1: X-ray patterns of (a) sugarcane bagasse ash calcined at 600 ℃ for 4 hours, (b) silica gel with Na_2SO_4 peaks and (c) pure silica powder.

(ii) X-ray analysis of chicken eggshell ($CaCO_3$) and CaO

Fig. 6.2 (a) represents the XRD diffracto graphs of raw chicken eggshells. The obtained peaks are well matched with standard ICDD card no. 01-086-2334. The major peak observed at $2\theta = 29.4^{\circ}$ reveals that eggshells are mainly composed of calcite ($CaCO_3$) [2]. On calcination, eggshells were completely transformed into calcium oxide (CaO) due to the removal of carbonate species. Fig. 6.2 (b) demonstrates the XRD pattern of calcium oxide extracted from chicken eggshells. The as-obtained peak values strongly match with the standard values corresponding to the ICDD card no. 00-048-1467. The absence of a peak at $\sim 2\theta = 29.4^{\circ}$ indicates the formation of pure CaO phase. No other impure phase related to calcium carbonate is observed. XRD spectra revealed sharp and narrow peaks which confirmed the presence of crystalline CaO.

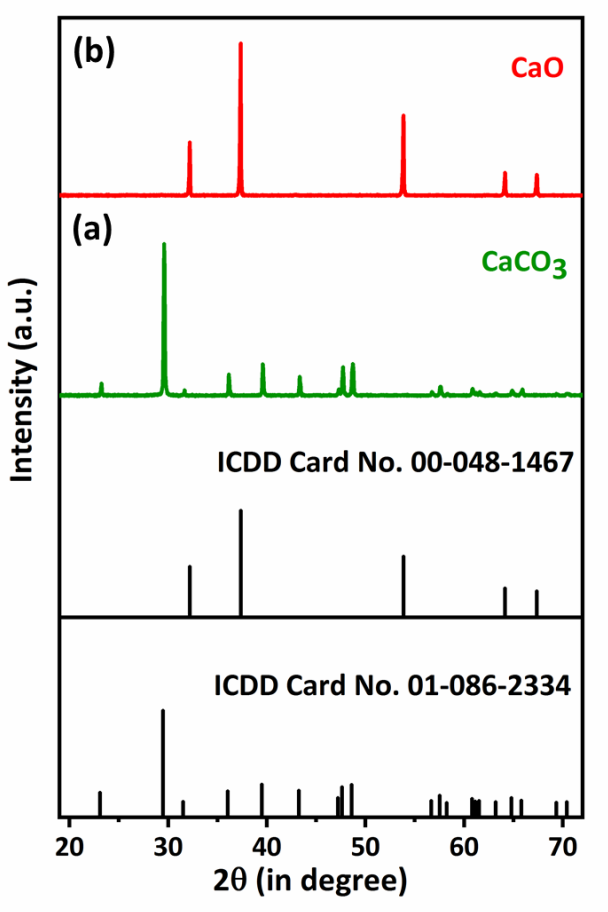

Figure 6.2: XRD pattern of (a) chicken eggshells and (b) calcium oxide.

(iii) X-ray analysis of undoped and Eu^{3+} doped Ca_2SiO_4 phosphors

The XRD patterns of agro-food waste derived undoped and Eu^{3+} (0.1-0.5 mol%) doped Ca_2SiO_4 phosphors are displayed in Fig. 6.3 (a - f). The acute peaks observed in the XRD spectra reveal the crystallinity of the synthesized phosphors. All the diffraction peaks are found to match perfectly with the ICDD card no. 01-083-0463. The as-synthesized phosphors presented monoclinic crystal structure. The obtained crystallographic lattice parameters are a = 5.5072 Å, b = 6.7511 Å, c = 9.3051 Å, α = 90.00º, β = 94.59º, γ = 90.00º with unit cell volume of 344.85 $Å^3$. No impure diffraction peaks corresponding to Eu_2O_3 (~2θ = 28.49º, ICDD card no. 03-065-3182) and other initial precursors are found in the XRD spectra of doped and undoped Ca_2SiO_4 phosphors. Eminently, the satisfactory percentage distinction in the ionic range of dopant and host element ought not surpass 30

%. The radius percentage difference (D_r) between host ions (Ca^{2+}) and doped ions (Eu^{3+}) in the $Ca_2SiO_4:Eu^{3+}$ phosphors is calculated using the following formula [3]:

$$D_r = \frac{R_h(CN) - R_d(CN)}{R_h(CN)} \times 100\% \quad (1)$$

where, CN represents the coordination numbers, R_h (CN) shows the cation radius and R_d (CN) shows the dopant radius. In case of β-Ca_2SiO_4, Ca^{2+} ions occupy two non-equivalent sites; Ca (I) and Ca (II) with 7 and 8 atoms of oxygen in the coordination spheres (Ca-O_7, Ca-O_8), respectively [4]. The ionic radii for Ca (I) and Ca (II) sites are 1.06 Å and 1.12 Å, respectively while, the ionic radius of Eu^{3+} for 7-coordinated and 8-coordinated are 1.11 Å and 1.06 Å, respectively. The acceptable percentage difference for 7-coordinated and 8-coordinated for β-$Ca_2SiO_4:Eu^{3+}$ is found to be 4.71 % and 4.82 %, respectively. Thus, it is believed that Ca^{2+} ions are replaced by Eu^{3+} ions at two non-equivalent sites [5]. Moreover, with the incorporation of Eu ions in Ca_2SiO_4, no prominent change in the XRD profile is observed. A small shifting in the XRD peak positions is observed with the incorporation of Eu ions. The crystallite size is determined by using Debye Scherrer's formula [6]:

$$D = \frac{0.9\,\lambda}{\beta \cos\theta} \quad (2)$$

where, D represents the crystallite size, λ shows the incident Cu K_α X-ray radiation wavelength (1.54 Å), β shows the full width at half maximum (FWHM) and θ is the Bragg's diffraction angle. β in equation (2) highly depends on the sample and instrumental effects which is corrected by the use of a standard sample of Si and determined using the following expression [7]:

$$\beta = \left\{\left(\beta_{experimental}\right)^2 - \left(\beta_{instrumental}\right)^2\right\}^{1/2} \quad (3)$$

The crystallite size is calculated to be around 40-60 nm. Doped samples displayed a little shifting of peaks as compared to the undoped sample.

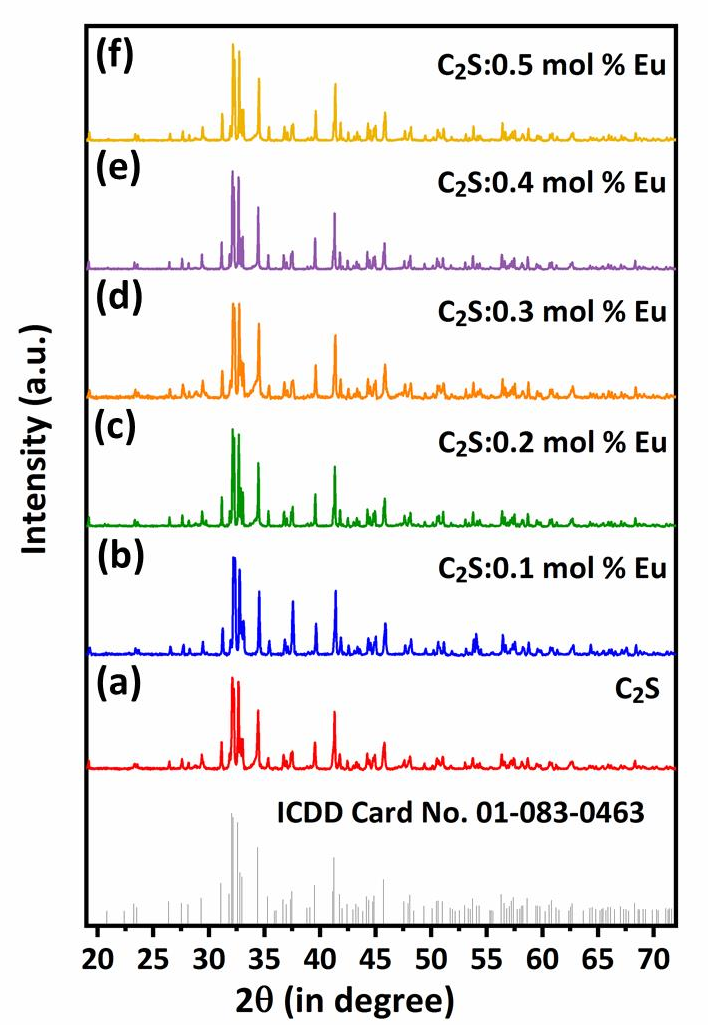

Figure 6.3: XRD spectra of undoped and Eu^{3+} activated Ca_2SiO_4 phosphors.

6.2. Fourier transform infrared (FTIR) Analysis

Fig. 6.4 (a) represents the FT-IR spectra of sugarcane bagasse ash derived silica. The broad spectra of synthesized silica in the region 2900-3700 cm^{-1} can be ascribed to the stretching vibrations of OH group corresponding to both silanol groups and adsorption of water [8]. The small band observed at 1639.4 cm^{-1} indicates the bending and stretching vibrations of adsorbed water molecules [9]. The presence of a band in the region 1102-1110 cm^{-1} is attributed to Si-O-Si asymmetric stretching [10,11]. The peak obtained at 619.8 cm^{-1} confirms the presence of Si-H vibrations [12]. The bands positioned at 799.4 and 471.2 cm^{-1} indicate the existence of Si-O-Si symmetric stretching and bending vibrations, respectively [13]. A strong peak is observed at 799.4 cm^{-1} which is

characteristic of amorphous silica [8]. This amorphous nature of obtained silica is in agreement with the XRD results.

Fig. 6.4 (b) demonstrates the FT-IR pattern of CaO powder extracted from the chicken eggshells. A wide band at 1458.2 cm^{-1} can be ascribed to carbonate symmetric stretching, which may be because of the presence of residual calcium carbonate [14]. Although no impure phase corresponding to $CaCO_3$ and $Ca(OH)_2$ are observed in CaO XRD pattern. The intense peak at 3641.4 cm^{-1} in the IR spectra represents the OH stretching vibration. The occurrence of the OH group is due to the absorption of moisture from the environment. The bands observed at 1056.4 cm^{-1} and 874.7 cm^{-1} demonstrates the absorption of carbon dioxide from the surrounding atmosphere during the experiment [15,16]. The appearance of a narrow band at 525.6 cm^{-1} depicts the Ca-O vibration [8,17]. Fig. 6.4 (c) and (d) represent the FT-IR spectra of as-synthesized pure and Eu activated Ca_2SiO_4 samples. Both pure and Eu activated samples presented similar IR spectra. The observed peaks in the range 3400-3600 cm^{-1} indicate the presence of OH stretching vibrations. No peak was observed in the region 1420-1460 cm^{-1} confirming the disappearance of free CaO phase in Ca_2SiO_4 phosphors. The occurrence of peaks at 996.5 and 845.7 cm^{-1} illustrates the symmetric stretching of Si-O-Ca bonds [18]. The Si-O-Si network linkage present in SiO_2 is broken due to the inclusion of calcium ions, which act as network modifiers. This leads to the emergence of Si-O stretching vibrations with one non-bridging silicon-oxygen (Si-O-non bridging oxygen). This distortion of the glassy network accounts for the formation of Si-O-Ca bonds [19]. The peak located at 888.9 cm^{-1} indicates Si-O asymmetric stretching vibrations, which is in correlation with the literature [20]. The depicted stretching vibrations specifies the presence of SiO_4^- group which exhibits tetrahedral structure. A sharp peak is observed at around 522.7 cm^{-1} which illustrates the O-Si-O bending [4]. The as-obtained IR and XRD results match appropriately. Therefore, the occurrence of peaks at around 996, 888.9, 845.7 and 522.7 cm^{-1} in Eu^{3+} activated powders confirms the formation of desired calcium orthosilicate (Ca_2SiO_4) phase.

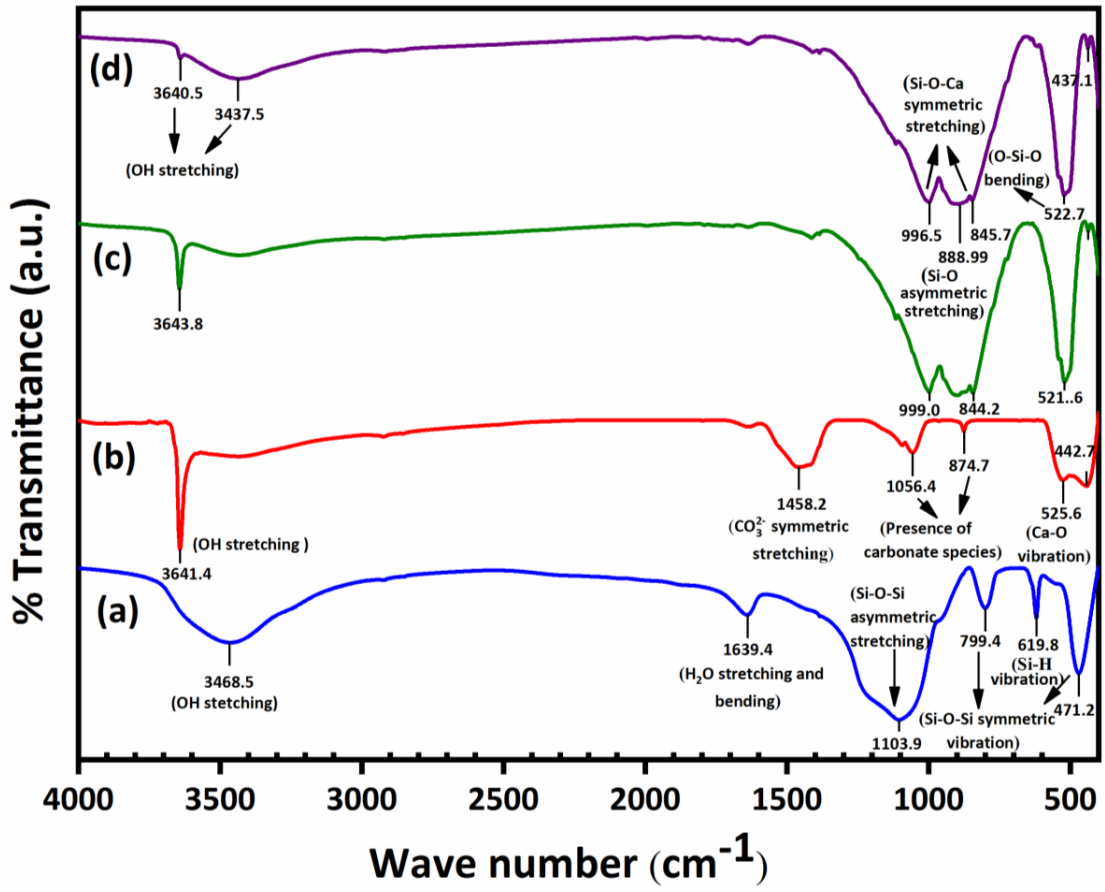

Figure 6.4: FT-IR vibrational spectra for the samples (a) SiO_2, (b) CaO, (c) Ca_2SiO_4 and (d) Ca_2SiO_4:0.4 mol % Eu^{3+}.

6.3. UV-Vis Spectroscopy

To have a better understanding of the effect of Eu doping on the optical properties of Ca_2SiO_4 phosphors, UV-Vis spectra are recorded. Fig. 6.5 represents the reflectance spectra of undoped and Eu^{3+} doped (0.1-0.5 mol %) Ca_2SiO_4 phosphors recorded in the range 200-800 nm. The presence of bands at around 300- 500 nm is due to the 4f- 4f transitions emerging from the $^7F_0$ ground level. The reflectance decreases with doping because of optical transitions occurring in the optical band gap.

.

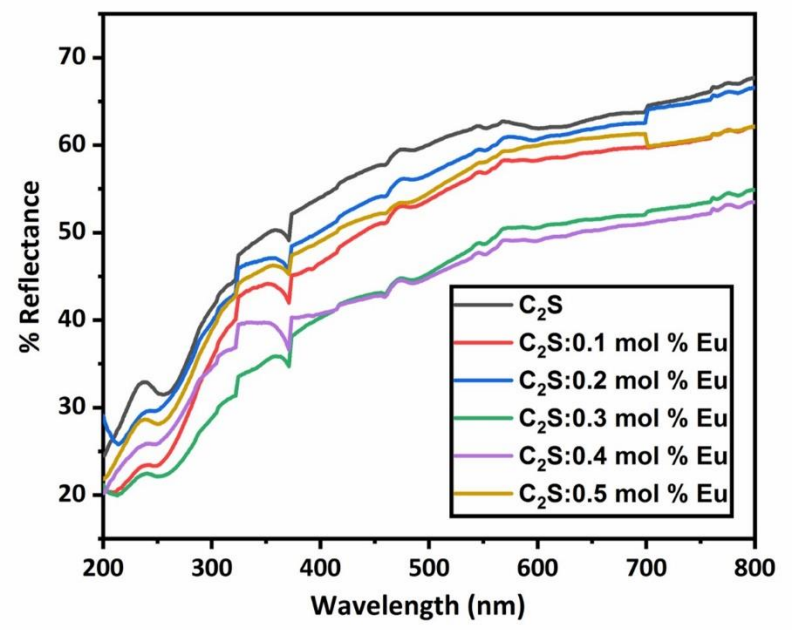

Figure 6.5: UV-vis reflectance spectra of undoped and 0.1-0.5 mol % Eu^{3+} doped Ca_2SiO_4 phosphors.

The band gap values of the as-synthesized phosphors were calculated with the help of the Kubelka-Munk (KM) theory. The Kubelka-Munk function F(R), which is a function of reflectance and directly proportional to absorbance can be written as [21]:

$$F(R) = \frac{(1-R)^2}{2R} \quad (4)$$

where, R represents the reflectance of the material. The relationship between the optical band gap (E_g) of the material and Kubelka-Munk function F(R) is as follows [22]:

$$F(R)h\nu = C\,(h\nu - E_g)^n \quad (5)$$

where, C is a constant, hν represents the photon energy and the value of n is 1/2, 2, 3/2, and 3 corresponding to the direct allowed, indirect allowed, direct forbidden and indirect forbidden transitions, respectively [23]. In accordance with the equation (5), the graph is sketched between $(F(R)h\nu)^2$ and hν (eV) for the band gap determination as shown in fig. 6.6. The band gap values are determined by extrapolation of the linear section of the curves to the energy axis where $(F(R)h\nu)^2 = 0$ [24].

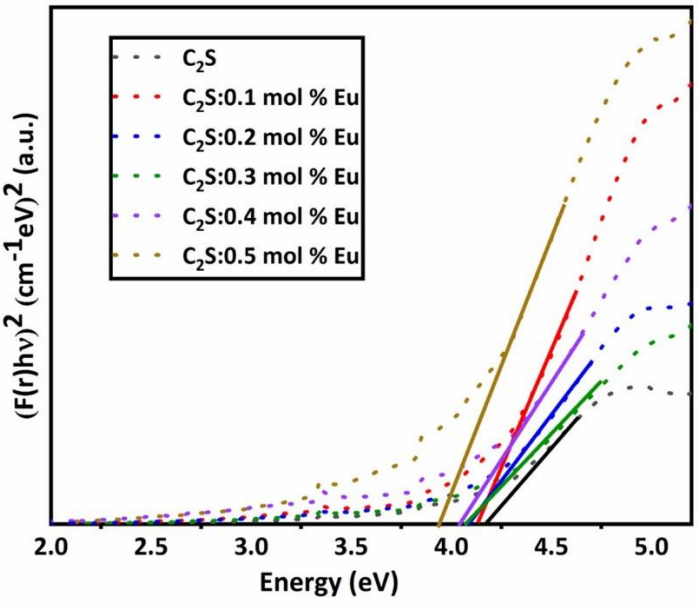

Figure 6.6: Kubelka-Munk plots of undoped and 0.1-0.5 mol % Eu^{3+} doped Ca_2SiO_4 phosphors.

The observed band gap for undoped and Eu doped Ca_2SiO_4 are tabulated in Table 6.1. It can be noticed that as the concentration of Eu^{3+} ions in the Ca_2SiO_4 host matrix increases, the band gap value decreases. Although the variation in the band gap is not much, still it can affect the optical properties for various applications in optoelectronic devices. This observed decrease in the band gap value can be associated with various reasons. The possible reason for the variation in the band gap can be linked to the extent of order-disorder of the lattice structure, which can affect the distribution of intermediary energy states due to the inclusion of Eu^{3+} dopant ions [25]. In case of multicomponent oxides, the broadness of the forbidden band of O 2p orbitals helps to estimate the position of the absorption band. The substitution of Ca^{2+} ions with Eu^{3+} ions may alter the structure of the band gap. This escalates the distortion degree of O 2p orbitals and the superpositioning of electron wave functions. As a result, the width of the optical band gap decreases. The other possible reason for the change in band gap values is due to the creation of oxygen vacancies ascribed to the imbalance of charge of Eu^{3+} and Ca^{2+} ions. The oxygen vacancies may lead to the generation of donor levels beneath the conduction band edge within the forbidden band gap and result in the decrease of the band gap in case of Eu doped samples [26].

Table 6.1: Band gap energy values of all the prepared Ca_2SiO_4 samples

Sample ID	Band gap energy E_g (in eV)
C_2S	4.16
C_2S: 0.1 mol% Eu	4.13
C_2S: 0.2 mol% Eu	4.08
C_2S: 0.3 mol% Eu	4.07
C_2S: 0.4 mol% Eu	4.03
C_2S: 0.5 mol% Eu	3.94

6.4. Elemental and morphological analysis

The sugarcane baggage ash (SCBA) was calcined at 600 ℃ and the presence of other metallic elements are analyzed by EDX spectra. Fig. 6.7 (a) represents the EDX spectra of SCBA containing other metallic elements along with silicon. The percentage compositions of all the obtained elements are tabulated in Table 6.2. The silicon content is found to be maximum than the other elements. This is in close agreement with the XRD patterns of SCBA which also represent the presence of various elements. The carbon content is also found to be significant in amount, which is further removed with alkali treatment and acidic precipitation. The gel-like silica obtained was further rinsed with D.I. water several times. The final product obtained was amorphous silica.

Table 6.2: Elemental composition of SCBA sample calcined at 600 ℃ (4 hrs)

Element	C	O	Na	Mg	Si	P	S	Cl	K	Ca	Fe
Weight %	21.55	32.36	0.98	1.22	31.64	1.61	0.38	0.06	6.38	3.66	0.17
Atomic %	33.49	37.74	0.79	0.94	21.02	0.97	0.22	0.03	3.04	1.70	0.06

The EDX spectrum of silica is shown in Fig. 6.7 (b) and reveals the presence of silicon and oxygen as major elements. The amorphous nature of silica obtained is confirmed by XRD and FTIR spectra. Fig. 6.7 (c) represents the EDX spectra of chicken eggshells and depicts the presence of carbon, calcium and, oxygen as major elements. The eggshells were calcined in order to get calcium oxide via decarbonization. Fig. 6.7 (d) represents the EDX spectra of calcium oxide. It can be illustrated from the spectra that it contains only two elements, oxygen and, calcium. No other elements related to carbon species are found in the spectra. This confirms the formation of pure calcium oxide from calcium carbonate.

Fig. 6.7 (e-f) represent the EDX spectra of undoped and europium doped Ca_2SiO_4 phosphors. The EDX spectrum confirms the presence of Eu element along with calcium, silicon and oxygen elements in doped samples as compared to undoped Ca_2SiO_4 sample.

.

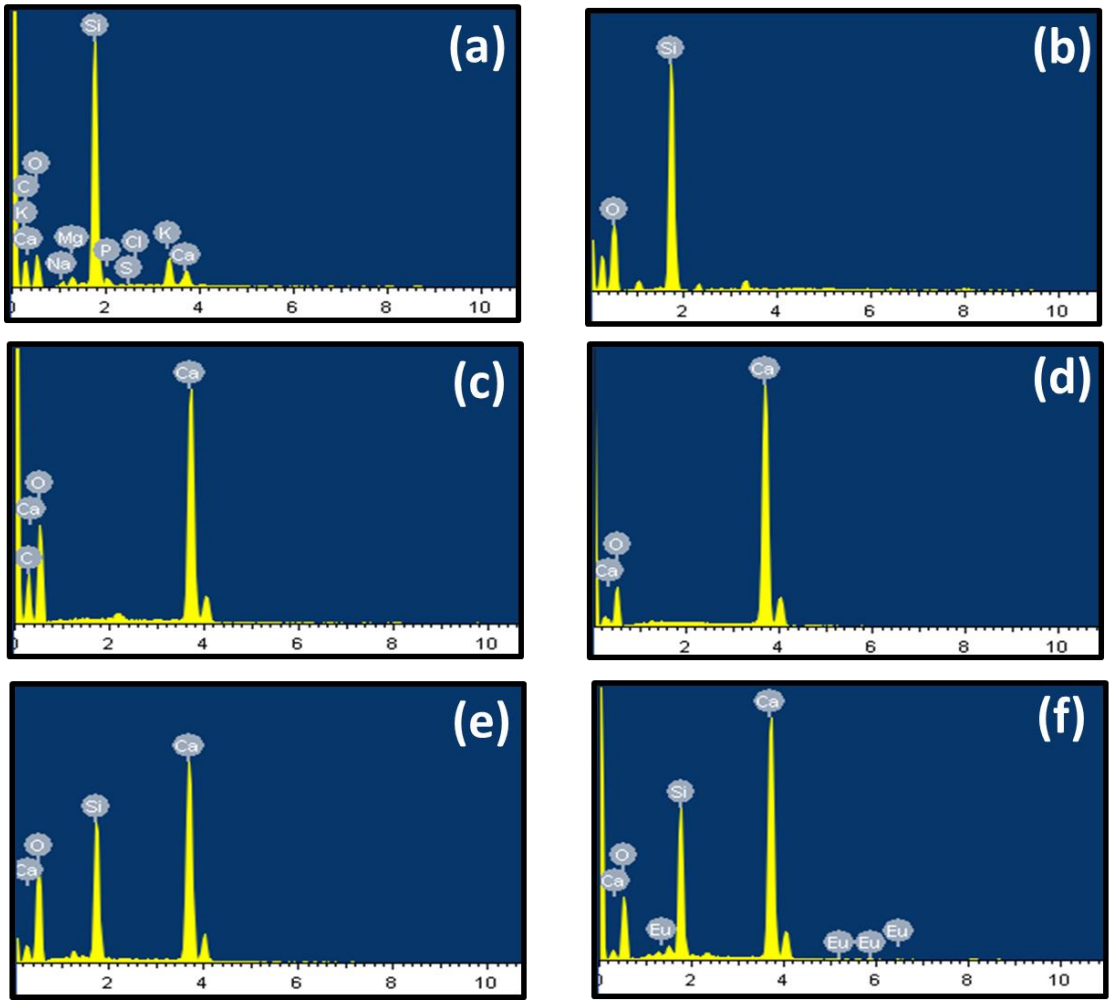

Figure 6.7: EDX spectra of (a) SCBA calcined at 600℃ (4 hrs), (b) SiO_2, (c) $CaCO_3$, (d) CaO, (e) Ca_2SiO_4 and (f) Ca_2SiO_4:0.4 mol % Eu^{3+}

The SEM micrographs of the undoped and Eu (0.1 to 0.5 mol%) doped Ca_2SiO_4 are shown in Fig. 6.8 (a - f). It is perceived that the particles exhibit irregular shape, non-uniform and agglomerated in nature. The non-uniform size distribution and agglomeration of the particles can also be observed as predicted in SEM images. Moreover, the particles have rounded edges which have advantages due to the greater density of packing, little light scattering and excellent luminescent features suitable for display applications.

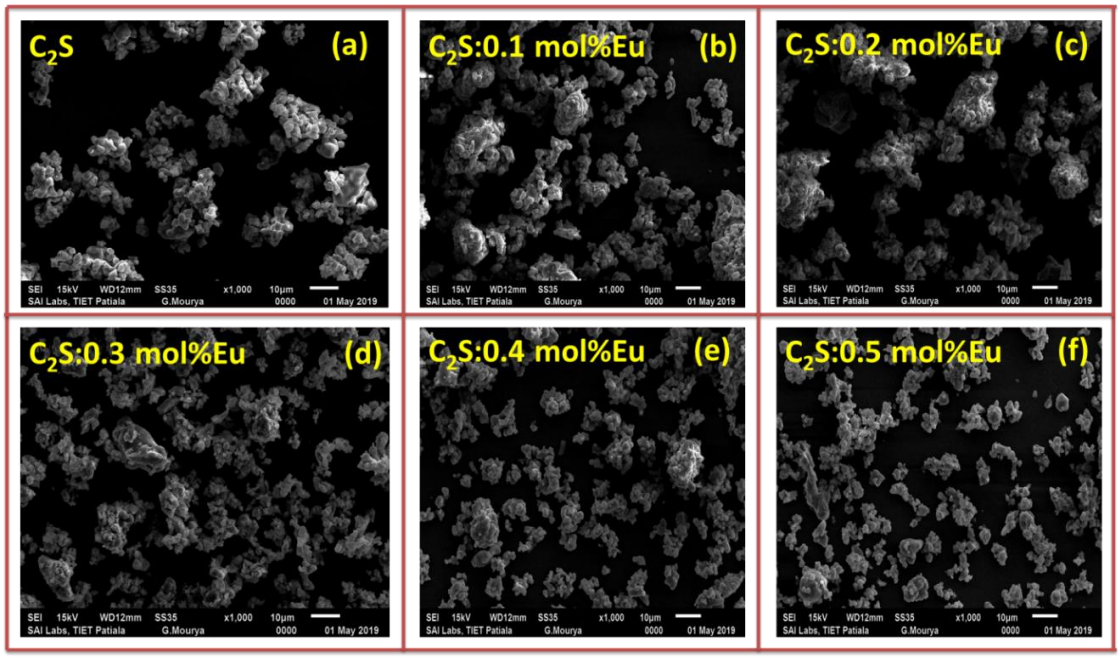

Figure 6.8: SEM micrographs of (a) undoped and (b-f) Eu^{3+} doped Ca_2SiO_4 phosphors.

6.5. Photoluminescence studies

The photoluminescence excitation spectra (PLE) of Eu^{3+} activated (0.1-0.5 mol %) Ca_2SiO_4 is shown in fig. 6.9. A record of excitation spectra was noted in the range 350-550 nm at wavelength 625 nm. The PLE spectra consist of several peaks ranging from near UV to visible region. The strongest peak obtained at 392 nm indicates the $^7F_0 \rightarrow {}^5L_6$ transitions of Eu^{3+} ions. A progression of various other peaks centered at 360, 380, 400 and 464 nm correspond to $^7F_0 \rightarrow {}^5L_{7,4,3,2}$ Eu^{3+} ion intra-configurational transitions, respectively [27]. It has been seen that varying concentration of Eu^{3+} ions in Ca_2SiO_4 lattice has not produced a significant effect on the shape and position of the peaks. However, the intensification of the band is seen with the escalating Eu^{3+} ions concentration. It is already determined that the highest intensity of excitation is observed for transition at 392 nm corresponding to $^7F_0 \rightarrow {}^5L_6$ transitions. Thus, near-UV light is appropriate for the excitation of these phosphors, which makes these agro-food waste synthesized phosphors useful in the construction of near-UV light-excited white light emitting diodes in solid-state lightening devices.

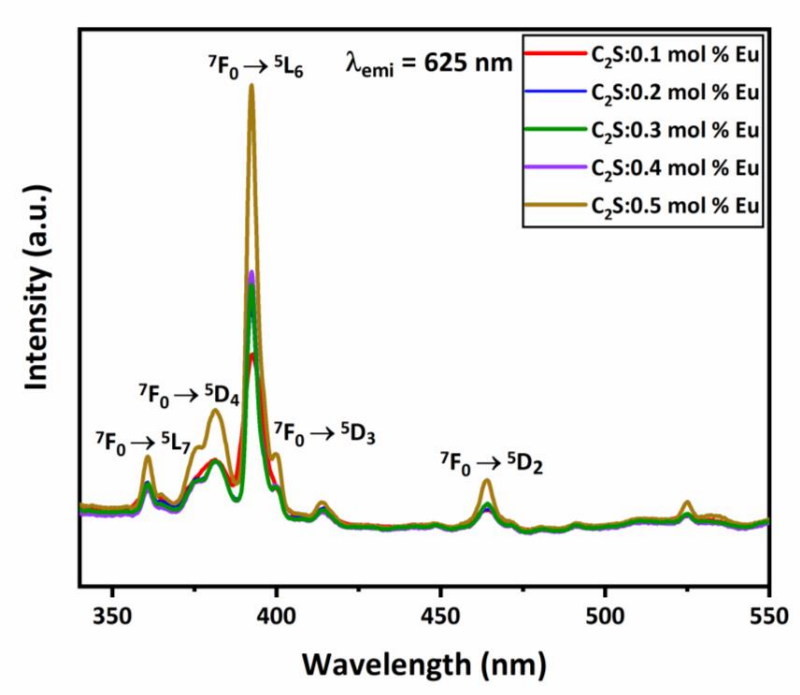

Figure 6.9: PL excitation spectra of $Ca_2SiO_4:Eu^{3+}$ (0.1-0.5 mol %) phosphors at λ_{emi} = 625 nm.

The emission spectra of $Ca_2SiO_4:Eu^{3+}$ (0.1-0.5 mol %) under 392 nm excitation in the range 550-750 nm is displayed in fig. 6.10. A number of emission peaks are observed at 580, 593, 615, 625, 653 and 705 nm attributed to $^5D_0 \rightarrow {}^7F_0$, $^5D_0 \rightarrow {}^7F_1$, $^5D_0 \rightarrow {}^7F_2$, $^5D_0 \rightarrow {}^7F_2$, $^5D_0 \rightarrow {}^7F_3$ and $^5D_0 \rightarrow {}^7F_4$ Eu^{3+} ion transitions, respectively [28]. Moreover, the $^7F_2$ level of Eu^{3+} ion splits into two well-resolved components due to crystal splitting. The emission peak centered around 593 nm corresponding to $^5D_0 \rightarrow {}^7F_1$ is a magnetic dipole transition and is inconsiderate to the symmetry of the site. The transition corresponding to $^5D_0 \rightarrow {}^7F_2$ is electric dipole and is also hypersensitive to the local domain of Eu^{3+} ions in the host lattice. When the Eu^{3+} dopant ions are present at inversion symmetry sites, the most dominant transition is $^5D_0 \rightarrow {}^7F_1$, whereas the occupancy at non-inversion symmetry sites leads to the $^5D_0 \rightarrow {}^7F_2$ transition.

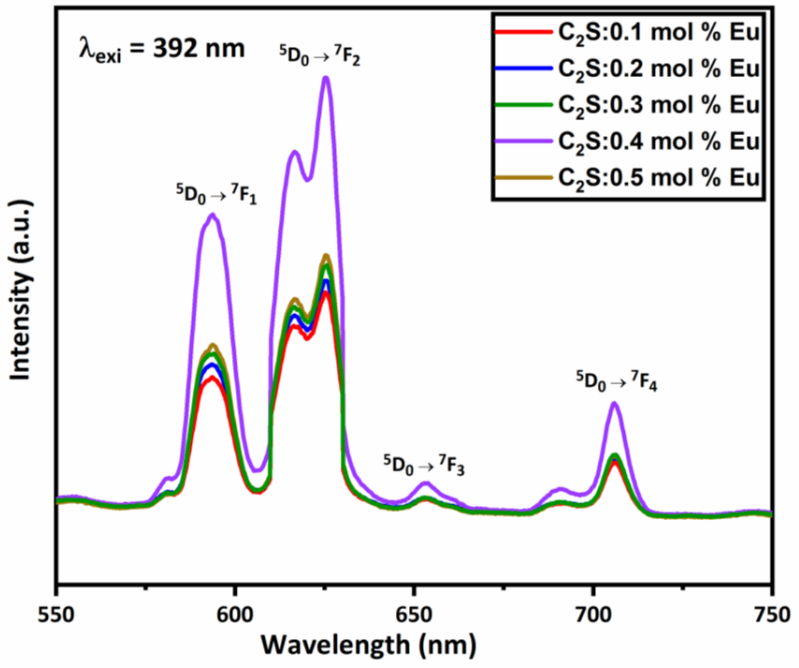

Figure 6.10: PL emission spectra of $Ca_2SiO_4:Eu^{3+}$ (0.1-0.5 mol %) phosphors at λ_{exc}=392 nm.

The asymmetric ratio (A_r), which is the ratio of $^5D_0 \rightarrow {}^7F_2$ to $^5D_0 \rightarrow {}^7F_1$ transition, is an important parameter to quantify the amount of deformation from the inversion symmetry of the neighborhood of the Eu^{3+} ions incorporated in the host structure [29]. The asymmetric ratio can be calculated as follows:

$$A_r = \frac{\int I_2(^5D_0 \rightarrow {}^7F_2)d\lambda}{\int I_1(^5D_0 \rightarrow {}^7F_1)d\lambda} \quad (6)$$

The dissimilarity of the asymmetric ratio due to the varying Eu^{3+} ion concentration is depicted in fig. 6.11 and the as-calculated values are formulated in Table 6.3. The asymmetric ratio increases up to 0.4 mol % of Eu^{3+} ion and then decreases. The decrease in the asymmetric ratio beyond 0.4 mol % of Eu ions is due to the presence of enhanced symmetrical surroundings around the dopant ions in the Ca_2SiO_4 host.

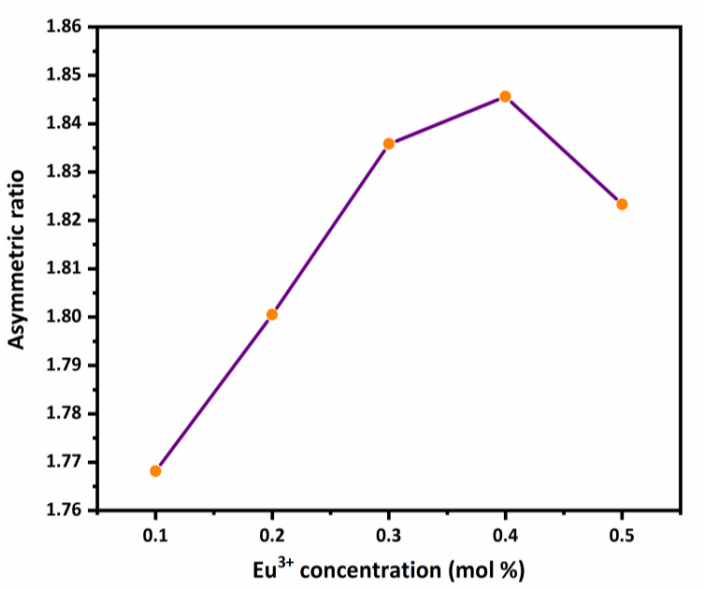

Figure 6.11: Effect of Eu^{3+} concentration on $^5D_0 \rightarrow {}^7F_2$/ $^5D_0 \rightarrow {}^7F_1$ ratio

The change of PL intensity with Eu ion concentration is also measured and shown in Fig. 6.12. It is observed that emission intensity increases with the increase in the concentration of Eu^{3+} ions and decreases beyond 0.4 mol % Eu^{3+} ions. The variation in the emission intensity corresponding to different transitions is shown in Fig. 6.12. The utmost intensity of emission is observed for 0.4 mol % Eu^{3+} ions in Ca_2SiO_4.

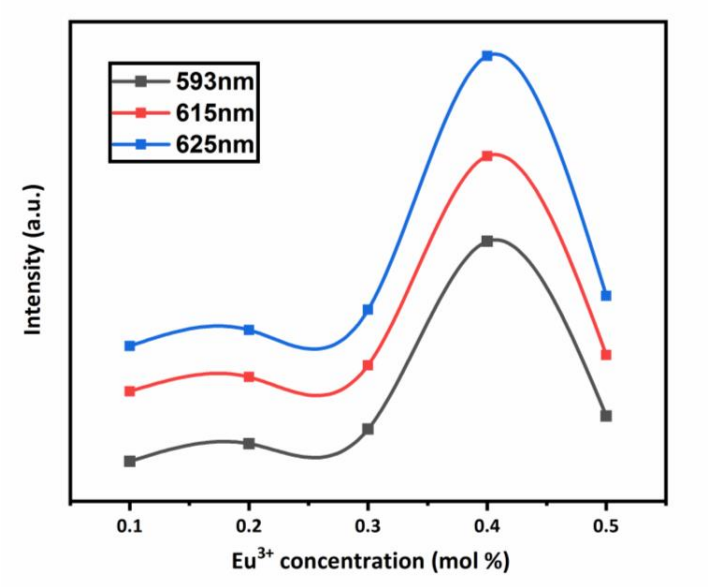

Figure 6.12: Variation in emission intensity with changing Eu^{3+} concentrations for transitions at 593, 615 and 625 nm wavelengths.

The systematic energy level distribution of emission and excitation spectra is highlighted in fig. 6.13. The increase in the emission intensity can be ascribed to various reasons. One of the possible reasons is that there are two Ca^{2+} sites in the Ca_2SiO_4, i.e., Ca (I) and Ca (II) in which calcium atoms form seven-fold (Ca-O_7) and eight-fold (Ca-O_8) octahedron with the oxygen atoms. The ionic radii of Ca and Eu are different in the different octahedron, which leads to the reduction in deformity of the crystal field surrounding the Eu^{3+} ions and enhancement in the luminous intensity.

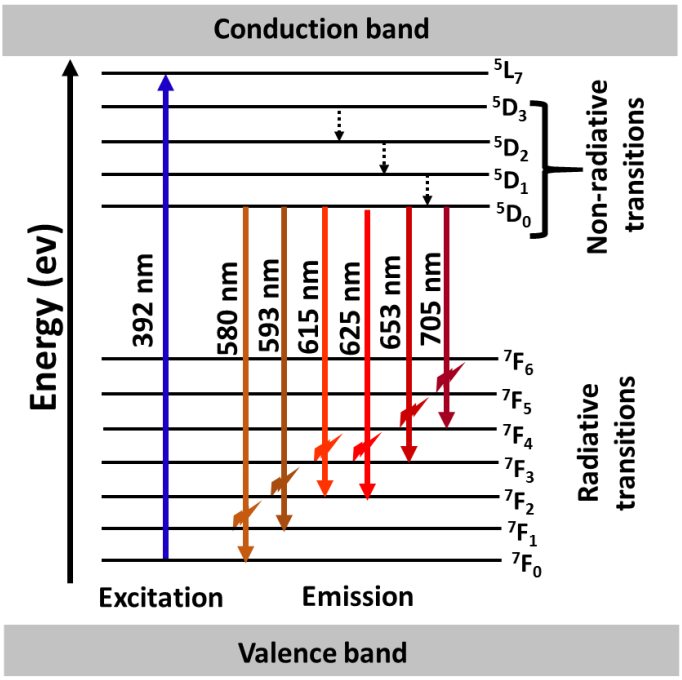

Figure 6.13: Energy level diagram of Eu^{3+} showing the luminescence mechanism

Moreover, there is an occurrence of imbalance of charge in the host cation (Ca^{2+}) and dopant ions (Eu^{3+}). When the Eu^{3+} ions substitute Ca^{2+} ions in Ca_2SiO_4, cation vacancies are created which can be represented as follows:

$$2Eu^{III} + 3Ca^{II} \rightarrow 2Eu^{x} + V_{Ca}^{x} \quad (7)$$

The formation of these oxygen vacancies serves as sensitizers and helps in luminescent enhancement. When the phosphors are excited under 392 nm, the restricted electron-hole pair strengthens the host excitation band. Further multiplication of the oxygen vacancies creates defects in the host lattice. The number of vacancies beyond a certain limit will lead to an efficient energy transfer from one activator to another, and then to imperfections,

which may act as a cause of luminescence quenching [30]. As a result, luminescent intensity decreases. Another major reason for the decrease in the luminescent intensity is the transmission of non-radiative energy among Eu^{3+} element which may be due to the multipole-multipole interaction, exchange interactions, or radiation reabsorption [31]. The increase in the Eu^{3+} ion concentration leads to the decrease in the minimal distance which is also called as the critical distance (R_c) among the Eu^{3+} ions. The value of the critical distance has been calculated using Blasse's theory. In accordance with Blasse's theory, if the R_c value is 5 Å or lower, exchange interaction leads to the non-radiative transmission and the value of R_c greater than 5 Å, leads to multipole-multipole interactions. If the Eu^{3+} ions solely replace the Ca^{2+} ions, and x_c represents the Eu^{3+} ion critical concentration, N numerates the Ca sites in the unit cells and V denotes the unit cell volume, then on an average one activator per ion $\left[\frac{V}{x_c N}\right]$volume is present. Then according to Blasse's rule, critical distance is nearly equivalent to double the radius of a sphere exhibiting this volume.

$$R_C = 2[\frac{3V}{4\pi x_c N}]^{1/3} \quad (8)$$

For Ca_2SiO_4:0.4 mol % Eu^{3+}, V = 344.85 $Å^3$, x = 0.004 and N = 4; results in a critical distance of 34.5 Å. The sort of interaction involved in the transfer of energy can be discovered with the use of Dexter and Schulman theory [32]. As per this theory, the PL emission intensity (I) per activator is expressed as:

$$\frac{I}{x} = \frac{K}{1+\beta(x)^{Q/3}} \quad (9)$$

where, x represents the activator concentration, K and β are constants ascribed to a certain interaction and the Q values may be 6, 8, or 10 and lower than 6 correspond to dipole-dipole, dipole–quadrupole, or quadrupole–quadrupole interactions and charge transfer mechanism, respectively. The slope of the graph (-Q/3), plotted log I/x vs log x (fig. 6.14) reveals the kind of interaction. For the present case, the slope of the graph is found to be -0.776 which leads to Q value 2.33, which is less than 6. Thus, it leads to the confirmation that cause of concentration quenching is energy transfer among the nearest neighboring ions i.e. exchange interactions.

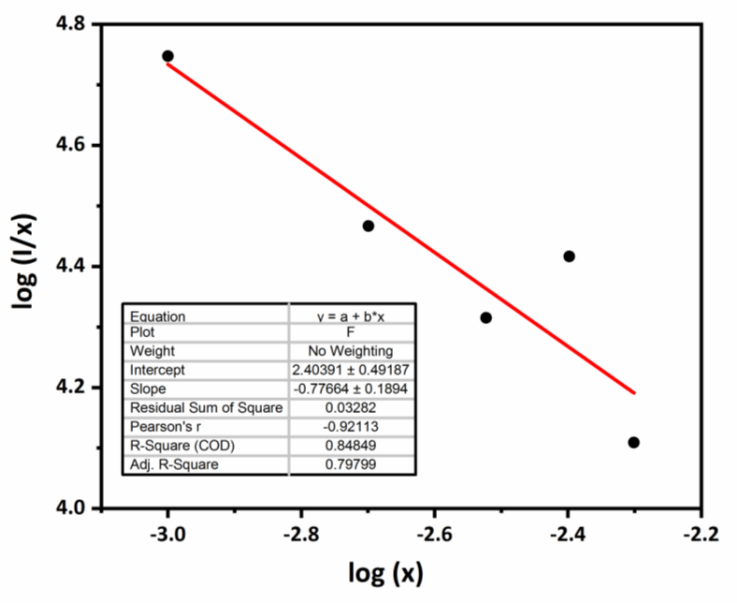

Figure 6.14: Graph of log I/x vs log x for $Ca_2SiO_4:Eu^{3+}$ (0.1-0.5 mol %)

The perception of the light emitted by the phosphors is determined using CIE (International Commission on Illumination) diagram. The CIE coordinates are determined using CIE calculator with the help of MATLAB (version R2016b) programme. Fig. 6.15 visualizes the CIE figure of the $Ca_2SiO_4:Eu^{3+}$ phosphors. The as-determined CIE coordinates of the synthesized samples capture the red domain. In accordance to National Television Standard Committee (NTSC), CIE coordinates for absolute red color are x = 0.67, y = 0.33. The calculated CIE coordinates of agro-food waste derived Ca_2SiO_4 phosphors lie close to the red region. Thus, these phosphors are efficient materials for optoelectronic devices for red light emission.

The correlated color temperature (CCT) values are estimated using the empirical formula formulated by McCamy. According to this approach [33]:

$$CCT = -437n^3 + 3601n^2 - 6861n + 5514.31 \quad (10)$$

where, $n = (x-x_e)/(y-y_e)$ and the chromaticity epicenters are at $x_e = 0.3320$ and $y_e = 0.1858$. The as-estimated CCT values lie in the range 1215-1311 K. CCT numeric value lower than 5000 K is suitable for warm white lightning mostly used for domestic appliances. Thus, these synthesized phosphors are useful for home lightening applications.

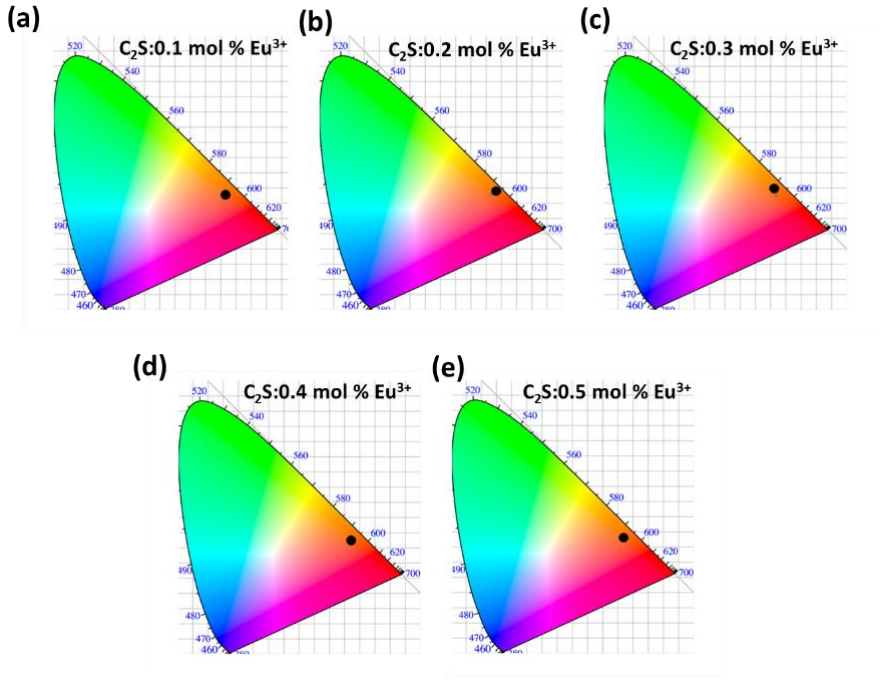

Figure 6.15: CIE coordinates of Ca_2SiO_4:x mol % Eu^{3+} phosphors a) x = 0.1, b) x = 0.2, c) x = 0.3, d) x = 0.4, and e) x = 0.5.

The red light emitted by the phosphors is investigated by the color purity of the prepared samples. Color purity is determined using the equation as follows [34]:

$$Color\ purity\ (\%) = \frac{\sqrt{(x-x_i)^2 + (y-y_i)^2}}{\sqrt{(x_d-x_i)^2 + (y_d-y_i)^2}} \times 100 \qquad (11)$$

where, (x, y) represent the color coordinates of the synthesized phosphor, (x_i, y_i) represents the CIE coordinates of white radiance and (x_d, y_d) are the CIE coordinates of the preeminent wavelength. The purity of color of the agro-food derived phosphors is found to be more than 80 % with a maximum value of 83.20 % for 0.4 mol % Eu^{3+} concentration.

Table 6.3: CIE coordinates, CCT values and color purity of Ca_2SiO_4:Eu^{3+} (0.1-0.5 mol %)

Phosphor	CIE Coordinates		CCT values (K)	Color purity (%)	Asymmetric ratio
	x	y			
C_2S:0.1 mol % Eu	0.6156	0.3838	1311	80.65	1.76
C_2S:0.2 mol % Eu	0.6162	0.3832	1306	80.78	1.80
C_2S:0.3 mol % Eu	0.6182	0.3812	1288	81.23	1.83
C_2S:0.4 mol % Eu	0.6268	0.3726	1215	83.20	1.84
C_2S:0.5 mol % Eu	0.6199	0.3795	1273	81.60	1.82

The calculated CIE coordinates, CCT values and color purity of $Ca_2SiO_4:Eu^{3+}$ phosphors are displayed in Table 6.3. It can be viewed that the obtained photometric parameters (CIE, CCT and color purity) are better than the values reported for phosphors which are synthesized via commercially available precursors [35–38]. Thus, it can be inferred that these agro-food waste derived phosphors can be successfully used for solid-state lightening devices for the manufacturing of near-UV excited (WLED's) white light emitting diodes.

REFERENCES

[1] C. Channoy, S. Maneewan, C. Punlek, S. Chirarattananon, Preparation and Characterization of Silica Gel from Bagasse Ash, Adv. Mater. Res. 1145 (2018) 44–48.

[2] S. Chraibi, H. Moussout, F. Boukhlifi, H. Ahlafi, M. Alami, Utilization of Calcined Eggshell Waste as an Adsorbent for the Removal of Phenol from Aqueous Solution, J. Encapsulation Adsorpt. Sci. 06 (2016) 132–146.

[3] M. Peng, Z. Pei, G. Hong, Q. Su, The reduction of Eu^{3+} to Eu^{2+} in $BaMgSiO_4$:Eu prepared in air and the luminescence of $BaMgSiO_4$:Eu^{2+} phosphor, J. Mater. Chem. 13 (2003) 1202–1205.

[4] R. Mani, H. Jiang, S.K. Gupta, Z. Li, X. Duan, Role of Synthesis Method on Luminescence Properties of Europium(II, III) Ions in β-Ca_2SiO_4: Probing Local Site and Structure, Inorg. Chem. 57 (2018) 935–950.

[5] E. Ozturk, E. Karacaoglu, The Effect of Ligand-To-Eu^{3+} Charge-Transfer Transitions (Lmct) on the Photoluminescence Intensity of M_2SiO_4: Eu^{3+} (M = Ca, Zn) Type Phosphors, Mater. Sci. Pol. 36 (2018) 509–513.

[6] R.A. Mir, O.P. Pandey, Influence of graphitic/amorphous coated carbon on HER activity of low temperature synthesized β -Mo_2C nanocomposites, 348 (2018) 1037–1048.

[7] N. Kaur, R.A. Mir, O.P. Pandey, Electrochemical and optical studies of facile synthesized molybdenum disulfide (MoS_2) nanostructures, J. Alloys Compd. 782 (2019) 119–131.

[8] S. Sompech, T. Dasri, S. Thaomola, Preparation and Characterization of Amorphous Silica and Calcium Oxide from Agricultural Wastes, Oriental Journal of Chemistry 32 (2016), 1923-1928.

[9] V. Vaibhav, U. Vijayalakshmi, S.M. Roopan, Agricultural waste as a source for the production of silica nanoparticles, Spectrochim. Acta - Part A Mol. Biomol. Spectrosc. 139 (2015) 515–520.

[10] N. Rahmat, M.A. Sabali, A.V. Sandu, N. Sahiron, I.G. Sandu, Study of Calcination Temperature and Concentration of NaOH Effect on Crystallinity of Silica from Sugarcane Bagasse Ash (SCBA), Rev. Chim. 67 (2016) 1872–1875.

[11] R.H. Alves, T.V.D.S. Reis, S. Rovani, D.A. Fungaro, Green Synthesis and Characterization of Biosilica Produced from Sugarcane Waste Ash, J. Chem. 2017 (2017) 1-9.

[12] R. Yuvakkumar, V. Elango, V. Rajendran, N. Kannan, High-purity nano silica powder from rice husk using a simple chemical method, J. Exp. Nanosci. 9 (2014) 272–281.

[13] P. Worathanakul, W. Payubnop, A. Muangpet, Characterization for Post-treatment Effect of Bagasse Ash for Silica Extraction, Int. J. Chem. Mol. Nucl. Mater. Metall. Eng. 3 (2009) 339–341.

[14] S. Ummartyotin, B. Tangnorawich, Utilization of eggshell waste as raw material for synthesis of hydroxyapatite, Colloid Polym. Sci. 293 (2015) 2477–2483.

[15] T. Andherson, D. Rachmat, D.D. Risanti, Potential use of chicken eggshells and

cacao pod husk as catalyst for biodiesel production, AIP Conf. Proc. 1945 (2018) 020058-1–020058-8.
[16] L.M. Correia, R.M.A. Saboya, N. de Sousa Campelo, J.A. Cecilia, E. Rodríguez-Castellon, C.L. Cavalcante, R.S. Vieira, Characterization of calcium oxide catalysts from natural sources and their application in the transesterification of sunflower oil, Bioresour. Technol. 151 (2014) 207–213.
[17] T. Witoon, Characterization of calcium oxide derived from waste eggshell and its application as CO_2 sorbent, Ceram. Int. 37 (2011) 3291–3298.
[18] M. Mansha, S.H. Javed, M. Kazmi, N. Feroze, Study of Rice Husk Ash as Potential Source of Acid Resistance Calcium Silicate, Adv. Chem. Eng. Sci. 01 (2011) 147–153.
[19] C.C. Chen, C.C. Ho, C.H. David Chen, S.J. Ding, Physicochemical Properties of Calcium Silicate Cements for Endodontic Treatment, J. Endod. 35 (2009) 1288–1291.
[20] S. Maheswaran, S. Kalaiselvam, S.K.S. Saravana Karthikeyan, C. Kokila, G.S. Palani, β-Belite cements (β-dicalcium silicate) obtained from calcined lime sludge and silica fume, Cem. Concr. Compos. 66 (2016) 57–65.
[21] S.P. Tandon, J.P. Gupta, Measurement of Forbidden Energy Gap of Semiconductors by Diffuse Reflectance Technique, Phys. Status Solidi. 38 (1970) 363–367.
[22] R. López, R. Gómez, Band-gap energy estimation from diffuse reflectance measurements on sol-gel and commercial TiO_2: A comparative study, J. Sol-Gel Sci. Technol. 61 (2012) 1–7.
[23] S. Punj, K. Singh, Blue-green light emitting inherent luminescent glasses synthesized from agro-food wastes, J. Mater. Sci. Mater. Electron. 30 (2019) 3871–3881.
[24] J. Sun, H. Wang, Y. Zhang, Y. Zheng, Z. Xu, R. Liu, Structure and luminescent properties of electrodeposited Eu^{3+} - doped CaF_2 thin films, Thin Solid Films. 562 (2014) 478–484.
[25] S. Jaidka, S. Khan, K. Singh, Na_2O doped CeO_2 and their structural, optical, conducting and dielectric properties, Phys. B Condens. Matter. 550 (2018) 189–198.
[26] M. Sahu, P. Biswas, Single-step processing of copper-doped titania nanomaterials in a flame aerosol reactor, Nanoscale Res. Lett. 6 (2011) 1–14.
[27] R.A. Barve, N. Suriyamurthy, B.S. Panigrahi, B. Venkatraman, Optical properties and Judd – Ofelt analysis of Eu^{3+}-activated calcium silicate, Phys. B Phys. Condens. Matter. 475 (2015) 156–161.
[28] L.L. Devi, C.K. Jayasankar, Spectroscopic investigations on high efficiency deep red-emitting Ca_2SiO_4:Eu^{3+} phosphors synthesized from agricultural waste, Ceram. Int. 44 (2018) 14063–14069.
[29] N. Jain, B.P. Singh, R.K. Singh, J. Singh, R.A. Singh, Enhanced photoluminescence behavior of Eu^{3+} activated $ZnMoO_4$ nano phosphors via Tb^{3+} co-doping for light emitting diode, J. Lumin. 188 (2017) 504–513.
[30] J. Li, Y. Wang, B. Liu, Influence of alkali metal ions doping content on photoluminescence of (Y, Gd) BO_3 : Eu red phosphors under VUV excitation, J. Lumin. 130 (2010) 981–985.
[31] M. Buijs, A. Meyerink, Received 23 September 1986 Accepted 9 December 1986, J. Lumin. 37. 37 (1987) 9–20.

[32] Y. Liu, G. Liu, J. Wang, X. Dong, W. Yu, Multicolor photoluminescence and energy transfer properties of dysprosium and europium-doped Gd_2O_3 phosphors, Elsevier Ltd, Journal of Alloys and Compounds, 649 (2015) 96-103.
[33] C.S. McCamy, Correlated Color Temperature as an Explicit Function of Chromaticity Coordinates, Color Research and Application 17 (1931) 142–144.
[34] S. Jeet, O.P. Pandey, Template-free synthesis route to monophasic $BaMgAl_{10}O_{17}$: Eu2+ with high luminescence efficiency, 750 (2018) 85–91.
[35] K. Mondal, P. Kumari, J. Manam, Influence of doping and annealing temperature on the structural and optical properties of $Mg_2SiO_4:Eu^{3+}$ synthesized by combustion method, Curr. Appl. Phys. 16 (2016) 707–719.
[36] S. Som, A.K. Kunti, V. Kumar, V. Kumar, S. Dutta, M. Chowdhury, S.K. Sharma, J.J. Terblans, H.C. Swart, Defect correlated fluorescent quenching and electron-phonon coupling in the spectral transition of Eu^{3+} in $CaTiO_3$ for red emission in display application, J. Appl. Phys. 115, 193101 (2014).
[37] D. V. Sunitha, H. Nagabhushana, S.C. Sharma, B.M. Nagabhushana, R.P.S. Chakradhar, Luminescent characteristics of Eu^{3+} doped di-calcium silicate nano-powders for white LEDs, J. Alloys Compd. 575 (2013) 434–443.
[38] S. Som, S. Das, S. Dutta, H.G. Visser, M.K. Pandey, P. Kumar, R.K. Dubey, S.K. Sharma, Synthesis of strong red emitting $Y_2O_3:Eu^{3+}$ phosphor by potential chemical routes: comparative investigations on the structural evolutions, photometric properties and Judd–Ofelt analysis, RSC Adv. 5 (2015) 70887–70898.

CHAPTER 7
CONCLUSION

A series of undoped and Eu^{3+} (0.1 to 0.5 mol%) doped Ca_2SiO_4 phosphors were triumphantly developed via solid-state technique using precursors derived from sugarcane baggage ash and chicken eggshells agro-food waste materials. The extracted silica from sugarcane baggage ash was amorphous in nature, while the CaO obtained from chicken eggshells was crystalline. XRD results confirmed the formation of single monoclinic phased Ca_2SiO_4 phosphors. EDX results exhibited the presence of elemental composition of different elements present in the precursors and synthesized materials. FTIR results supported the formation of the silicate structure of agro-food waste derived calcium silicates. The as-synthesized phosphors emitted red light color under near UV excitation at 393 nm. The concentration quenching was found to be 0.4 mol% for Eu^{3+} ions in the host lattice. The critical distance was found to 34.5 Å and the interaction responsible for luminescence quenching was energy transfer interactions. CIE coordinates of the synthesized phosphors were found to lie in the red zone. The CCT values are found to be less and color purity above 80%, which are found to be better than many commercial precursors synthesized phosphors. The present report elucidates a simple, novel, economic and facile approach to synthesize Ca_2SiO_4:Eu phosphors. The as-synthesized phosphors can be used as luminescent material for the fabrication of near-UV excited white light emitting diodes, solid state lighting and, optoelectronic devices.

CHAPTER 8
FUTURE SCOPE

8.1. Suggestions for future work

The work done in this dissertation has opened a pathway to several research proposals which can be pursued further. These are listed as follows:

i. An attempt has been made to synthesize calcium silicate phosphors from agro-food wastes. In the present study, Ca_2SiO_4 is chosen as a host matrix. Similarly, other calcium silicates like $CaSiO_3$ and $Ca_3Si_2O_7$ can also be studied.

ii. Here, the research deals with the trivalent europium ion Eu^{3+} as the dopant material. Other efficient calcium silicate phosphors can also be synthesized by the employment of several rare earth dopant ions like Sm^{3+}, Dy^{3+}, Tb^{3+}, Eu^{2+}, etc.

iii. In the present study, sugarcane bagasse ash and chicken eggshells have been used as agro-food waste materials to synthesize calcium silicate phosphors. Other fine sources of silica such as bamboo leaves, bamboo culm, corn cob and, groundnut shell, while crab and duck shell for calcium oxide can also be used to synthesize calcium silicates.

Ishita Khurana MSc Thesis V01

ORIGINALITY REPORT

7%	2%	5%	5%
SIMILARITY INDEX	INTERNET SOURCES	PUBLICATIONS	STUDENT PAPERS

PRIMARY SOURCES

1	Submitted to Universiti Teknologi Malaysia Student Paper	1%
2	Kanchan Mondal, Dhananjay Kumar Singh, J. Manam. "Spectroscopic behavior, thermal stability and temperature sensitivity of Ca 2 SiO 4 : Eu 3+ red emitting phosphor for solid state lighting application", Journal of Alloys and Compounds, 2018 Publication	1%
3	Submitted to Jawaharlal Nehru Technological University Anantapur Student Paper	<1%
4	doaj.org Internet Source	<1%
5	Venkataravanappa, M., H. Nagabhushana, G.P. Darshan, B. Daruka Prasad, G.R. Vijayakumar, H.B. Premkumar, and Udayabhanu. "Novel EGCG assisted ultrasound synthesis of self-assembled Ca2SiO4:Eu3+ hierarchical superstructures: Photometric characteristics	<1%